

Gö-VIP-19: Dr. Ramona Schulz-Heddergott

Name der Einrichtung: Institut für Molekulare Onkologie

Titel der Publikation: Therapeutic ablation of gain-of-function mutant p53 in colorectal cancer inhibits Stat3-mediated tumor growth and invasion

In: Cancer Cell 34, 298–314, August 13, 2018, impact factor 22,8

Autoren:

1. Ramona Schulz-Heddergott
2. Nadine Stark
3. Shelley J. Edmunds
4. Jinyu Li
5. Lena-Christin Conradi
6. Hanibal Bohnenberger
7. Fatih Ceteci
8. Florian R. Greten
9. Matthias Dobbelstein*
10. Ute M. Moll*

(1, 2, 3, 9, 10) Institute of Molecular Oncology, University Medical Center Göttingen, 37077 Göttingen, Germany

(4, 10) Department of Pathology, Stony Brook University, Stony Brook NY 11794, USA

(5) Department of General, Visceral, and Pediatric Surgery, University Medical Center Göttingen, 37075 Göttingen, Germany

(6) Department of Pathology, University Medical Center Göttingen, 37075 Göttingen, Germany

(7, 8) Institute for Tumor Biology and Experimental Therapy, Georg-Speyer-Haus, 60596 Frankfurt/Main, Germany

* shared corresponding senior authorship

Zusammenfassung des wissenschaftlichen Inhalts

(Ramona Schulz-Heddergott)

Tumore des Darms sind von der häufigsten Mutante des Tumorsuppressorgens p53, mutp53-R248Q/W, abhängig. Diese Mutante fördert Wachstum und Ausbreitung der Tumore.

Wildtypisches p53 (wtp53) schützt uns vor Krebs. Mutp53-R248Q/W hat die gegenteilige Wirkung, weil hier nicht nur die tumorsuppressorische Wirkung von wtp53 aufgehoben wird, sondern mutp53-R248Q/W komplett neue, tumorfördernde Eigenschaften erhält. Das mutp53-R248Q/W Protein bringt diese gefährlichen Eigenschaften u.a. durch seine Stabilisierung durch das HSP90 System mit, ein System, was ebenfalls für seine tumorfördernden Eigenschaften bekannt ist. Andere Mutanten von p53 zeigen nicht diese

starke Stabilisierung, was wiederum die mutp53-R248Q/W Variante besonders gefährlich macht.

In einem präklinischen Mausmodell für Dickdarmkrebs konnten wir zeigen, dass eine genetische Wegnahme von mutp53-R248Q/W aus bereits entstandenen Tumoren deren Wachstum und Ausbreitung stark reduziert. Durch eine pharmakologische Behandlung mit einem Hsp90-Inhibitor wurde mutp53-R248Q/W in Tumoren abgebaut und das Tumorstadium so eingeschränkt. Mechanistisch gesehen fördert stabilisiertes mutp53-R248Q/W das Krebswachstum durch eine Überaktivierung von Stat3 (engl. signal transducer and activator of transcription 3), einem wichtigen wachstumsfördernden Transkriptionsfaktor. Stat3 wird direkt von mutp53-R248Q/W gebunden, welches dadurch nicht mehr de-phosphoryliert und somit inaktiviert werden kann. Das verstärkt den Signalweg von Stat3 und führt zu erhöhtem Tumorzellwachstum. Wird aber umgekehrt mutp53-R248Q/W abgebaut, so lässt auch die Stat3 Aktivität nach. Diese Ergebnisse können auch auf Patienten übertragen werden. Tumorproben von Dickdarmpatienten mit einer mutp53-R248Q/W Mutation zeigen eine höhere Stat3 Aktivität, und diese Patienten hatten eine schlechtere Überlebensrate.

Die häufigste p53 Mutante, mutp53-R248Q/W, ist über Hsp90 angreifbar. Die Inhibition von Hsp90 führt zum Abbau von mutp53-R248Q/W und stellt damit eine Therapiemöglichkeit für Darmkrebs dar. Da einige Hsp90-Inhibitoren bereits in klinischen Studien an anderen Tumorarten getestet werden, legen unsere Ergebnisse solche Studien auch für Dickdarmkrebs nahe. Insbesondere Patienten mit einer p53-R248Q/W Mutation könnten von einer Therapie mit Hsp90 Inhibitoren profitieren. Somit könnten unsere Ergebnisse die Basis für eine individuelle Therapie bei Darmkrebs darstellen.

Die Ergebnisse wurden am 13. August 2018 in der renommierten Fachzeitschrift Cancer Cell veröffentlicht.

Weitere Informationen:

Universitätsmedizin Göttingen

Institut für Molekulare Onkologie

Dr. Ramona Schulz-Heddergott,

Anschrift: Justus von Liebig Weg 11, 37077 Göttingen

Email: ramona.schulz@zentr.uni-goettingen.de

Telefon: 0551/39-33576

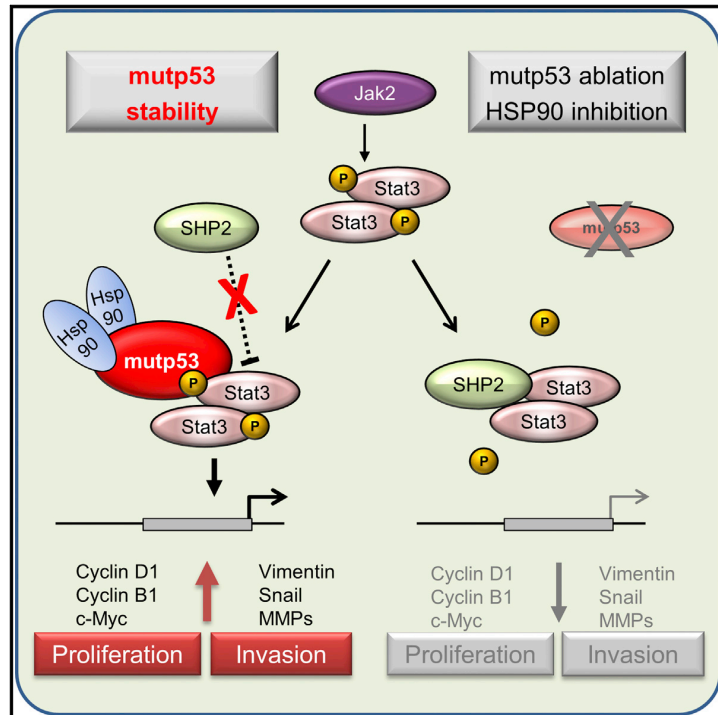


v.L.n.R.: Dr. Dr. Lena-Christin Conradi, Dr. Ramona Schulz-Heddergott und Dr. Hanibal Bohnenberger, alle Mitglieder des translationalen Else Kröner Forschungskollegs Göttingen und Autoren bzw. Ko-Autoren dieser Publikation.

Cancer Cell

Therapeutic Ablation of Gain-of-Function Mutant p53 in Colorectal Cancer Inhibits Stat3-Mediated Tumor Growth and Invasion

Graphical Abstract



Authors

Ramona Schulz-Heddergott,
Nadine Stark, Shelley J. Edmunds, ...,
Florian R. Greten,
Matthias Dobbelstein, Ute M. Moll

Correspondence

mdobbel@uni-goettingen.de (M.D.),
ute.moll@stonybrook.edu (U.M.M.)

In Brief

Schulz-Heddergott et al. show that the most common p53 mutant R248Q (mtp53) enhances Stat3 activation by binding to Stat3 and displacing SHP2 in colorectal cancer cells. Reduction of mtp53 genetically or by using the HSP90 inhibitor 17AAG reduces Stat3 signaling and the growth of mtp53-driven tumors.

Highlights

- mtp53 R248Q, the most common p53 mutant in human CRC, promotes CRC in mice
- mtp53 R248Q binds to and deregulates Stat3, correlating with poor patient survival
- Genetic ablation of mtp53 R248Q reduces growth and invasion of established CRCs
- Hsp90 inhibition reduces the mtp53 R248Q level and inhibits CRC progression



Therapeutic Ablation of Gain-of-Function Mutant p53 in Colorectal Cancer Inhibits Stat3-Mediated Tumor Growth and Invasion

Ramona Schulz-Heddergott,¹ Nadine Stark,¹ Shelley J. Edmunds,¹ Jinyu Li,² Lena-Christin Conradi,³ Hanibal Bohnenberger,⁴ Fatih Ceteci,⁵ Florian R. Greten,⁵ Matthias Dobbelstein,^{1,6,*} and Ute M. Moll^{1,2,6,7,*}

¹Institute of Molecular Oncology, University Medical Center Göttingen, Göttingen 37077, Germany

²Department of Pathology, Stony Brook University, Stony Brook, NY 11794, USA

³Department of General, Visceral, and Pediatric Surgery, University Medical Center Göttingen, Göttingen 37075, Germany

⁴Department of Pathology, University Medical Center Göttingen, Göttingen 37075, Germany

⁵Institute for Tumor Biology and Experimental Therapy, Georg-Speyer-Haus, Frankfurt am Main 60596, Germany

⁶Senior author

⁷Lead Contact

*Correspondence: mdobbel@uni-goettingen.de (M.D.), ute.moll@stonybrook.edu (U.M.M.)

<https://doi.org/10.1016/j.ccell.2018.07.004>

SUMMARY

Over half of colorectal cancers (CRCs) harbor *TP53* missense mutations (mutp53). We show that the most common mutp53 allele R248Q (p53^Q) exerts gain of function (GOF) and creates tumor dependence in mouse CRC models. mutp53 protein binds Stat3 and enhances activating Stat3 phosphorylation by displacing the phosphatase SHP2. Ablation of the p53^Q allele suppressed Jak2/Stat3 signaling, growth, and invasiveness of established, mutp53-driven tumors. Treating tumor-bearing mice with an HSP90 inhibitor suppressed mutp53 levels and tumor growth. Importantly, human CRCs with stabilized mutp53 exhibit enhanced Jak2/Stat3 signaling and are associated with poorer patient survival. Cancers with *TP53*^{R248Q/W} are associated with a higher patient death risk than are those having nonR248 mutp53. These findings identify GOF mutp53 as a therapeutic target in CRC.

INTRODUCTION

Colorectal cancer (CRC) is the third leading cause of cancer deaths worldwide. Loss of the powerful p53 tumor suppressor typically occurs at the critical transition from benign adenoma to invasive carcinoma, enabling invasion (Levine and Oren, 2009). Next to *APC*, *TP53* mutations are the second most common alteration in sporadic CRC, affecting ~60% of cases. Specifically, substitutions at residues R175, R248, and R273 within the DNA binding domain are the most frequent p53 alterations in CRC. Of R248 substitutions, over 90% are either Q or W, with similar frequencies (Cancer Genome Atlas Network, 2012).

Trp53 ablation specifically in murine intestinal epithelial cells alone is insufficient to initiate CRC, but strongly enhances tumor incidence and invasiveness after treatment with the carcinogen azoxymethane (AOM) (Schwitalla et al., 2013). Thus, p53 loss contributes to CRC, thereby faithfully modeling the human system. In addition to losing their tumor suppressor function, many of the p53 missense mutants (mutp53) actively promote cancer by acquiring gain-of-function (GOF) activities (Muller and Vousden, 2014). mutp53 GOF knockin mice exhibit shorter overall survival and/or more metastasis and a broader tumor spectrum than *Trp53-null* littermates (Hanel et al., 2013; Lang et al., 2004; Olive et al., 2004). Li-Fraumeni syndrome (LFS) patients with *TP53* missense mutations develop cancers earlier

Significance

GOF missense mutp53 proteins are stabilized by HSP90 and are often overexpressed in CRC but their contribution to *in vivo* cancer progression and possible therapeutic exploitability are unknown. We show that established mouse CRC driven by the hotspot GOF mutp53 R248Q depends on continued mutp53 expression to sustain high Jak2/Stat3 signaling in tumor cells for their growth and invasion. CRC with stabilized mutp53 exhibit enhanced Jak2/Stat3 signaling and are associated with poorer patient survival. Moreover, many cancer entities, including gastrointestinal, with *TP53*^{R248Q/W}, are associated with poorer patient survival versus those having nonR248 mutp53. Our data suggest that p53 GOF mutants in CRC represent actionable drug targets responsive to treatment with HSP90 inhibitors.



than LFS patients with p53 loss. Strikingly, $TP53^{R248Q/+}$ LFS patients have higher tumor numbers and shorter tumor-free survival compared with $TP53^{+/-}$ LFS patients (Hanel et al., 2013).

mutp53 proteins undergo stabilization specifically in tumors, a key feature and prerequisite of GOF (Hanel et al., 2013). The HSP90/HDAC6 chaperone machinery, which is ubiquitously activated in cancer compared with normal tissues (Whitesell and Lindquist, 2005), is a major determinant of mutp53 stabilization by providing protection from degradation by E3 ubiquitin ligases such as Mdm2 and CHIP (Blagosklonny et al., 1996; Li et al., 2011a, 2011b; Whitesell et al., 1998). In the context of T cell lymphomas we recently showed that GOF mutp53 is an actionable cancer-specific target. Spontaneous lymphomas developed by humanized p53 R248Q ($p53^Q$) and R172H ($p53^H$) knockin mice showed dependence on continued overexpression of mutp53 for tumor maintenance and metastasis. Conversely, its genetic ablation or pharmacological depletion with Hsp90 inhibitors caused regression or stagnation of transplanted and autochthonous lymphomas, and markedly extended animal survival (Alexandrova et al., 2015).

These findings raise the important question of whether targeting GOF mutp53 in epithelial cell-derived carcinomas, which comprise the vast majority of all human malignancies (~90%), would equally translate to therapeutic gains.

RESULTS

mutp53 Exerts GOF Activity in AOM/DSS-Induced and Mutant *Apc*-Mediated Mouse Models of Intestinal Cancer

The impact of mutant p53 on CRC was tested in two mouse models. The murine *Trp53* is abbreviated by “p53” from here on, and a deletion of *Trp53* is indicated by a minus sign (–) when used along with another allele. Otherwise it is designated as “p53-null” allele.

Apc mutant mice, including those harboring the *Apc*^{1638N} allele, represent the classic genetic intestinal tumor model, mirroring the human adenomatous polyposis coli (APC) syndrome (Fodde et al., 1994). To test whether the humanized mutp53 R248Q allele ($TP53^{R248Q}$, short “p53^Q”) exerts GOF in intestinal cancer, we combined this allele with either p53 wild-type (WT) (+) or KO (–) alleles. We compared 25-week-old p53^{Q/+}; *Apc*^{1638N/+} with p53^{-/+}; *Apc*^{1638N/+} mice and saw clear GOF activity over the p53-null allele with significantly higher tumor numbers and larger tumor sizes (Figure S1A), translating to shorter life expectancy by 10 weeks (Figure S1B). Similar GOF was observed comparing p53^{Q/+}; *Apc*^{1638N/+} with p53^{-/+}; *Apc*^{1638N/+} genotypes at 16 weeks, although only tumor size but not tumor numbers reached statistical significance (Figure S1C).

However, given that the overwhelming site of tumor development in *Apc* mutant mice is the small intestine, they are not the ideal model of human CRC, which affects the colon with a predilection for rectum and distal colon. Instead, the classic selective colorectal cancer model in mice entails a single exposure to the DNA methylating carcinogen AOM, combined with one cycle of dextrane sodium sulfate (DSS) to promote transient colitis. The AOM/DSS model has high penetrance and mirrors human CRC at the pathological and molecular level (Tanaka et al., 2003).

Tumors are strictly limited to colon, mostly to the distal colon. AOM induces mutations in *Ctnnb1* and *Kras* to constitutively activate the Wnt and mitogen-activated protein kinase pathways, respectively (De Robertis et al., 2011), but typically does not induce mutations in p53 (De Robertis et al., 2011; Schwitalla et al., 2013; Tanaka et al., 2003). However, genetic ablation of p53 enhances tumor formation in the AOM/DSS model (Figure S1D), as reported (Fujii et al., 2004).

Importantly, as already seen in the *Apc*^{1638N} model, the p53^Q allele again exerted GOF activity in the AOM/DSS model, indicated by an increase in tumor numbers and sizes, and by p53 stabilization (Figures 1A–1D). The heterozygous p53^{Q/+} genotype failed to show GOF (Figures S1E and S1F), likely because the 12-week endpoint after AOM was too short to allow more Q tumors to form compared with p53^{-/+} controls. In this short time frame the retained WT p53 allele likely exerted a “dominant positive” tumor suppressor function over the p53^Q allele, reflected by a widespread lack of mutp53 stabilization, with only focal accumulation (Figure 1D, compare p53^{Q/+} with p53^{Q/-}). In contrast, the extended 25-week endpoint used in p53^{Q/+}; *Apc*^{1638N/+} mice did allow the p53^Q allele to become dominant and execute GOF by imposing loss-of-heterozygosity (LOH) of the WT p53 allele (Figures S1A and S1B). An important determinant of GOF is the tumor-specific stabilization of mutp53 protein. Stabilization, in addition to Hsp90, also depends on LOH (Alexandrova et al., 2017), as indicated by circumscribed regions with mutp53 stabilization in p53^{Q/+} AOM/DSS and *Apc*^{1638N} tumors (Figures 1D and S1G). In sum, since the p53^Q allele exerts GOF in the AOM/DSS model that mirrors human CRC, we focused on the latter in this study.

Genetic Ablation of the Hotspot GOF mutp53 Allele Inhibits Tumor Growth

To test whether GOF mutp53 represents an important anti-tumor target in CRC *in vivo*, we used conditional mutp53 inactivation in our humanized floxed mutp53 R248Q ($TP53^{R248Q/flox}$, short “p53^{floxQ}”) knockin model. We crossed to *Rosa26CreERT2* (“ERT2”) mice to generate Tamoxifen-deletable p53^{floxQ/-}; ERT2 mice with corresponding controls (Alexandrova et al., 2015). To assess whether colonic tumors exhibit dependence on continuous high levels of mutp53, we first induced tumors and then deleted mutp53 via tamoxifen (TAM). To this end, we challenged p53^{floxQ/-}; ERT2 mice with AOM/DSS followed by serial colonoscopies. At 5 weeks after AOM/DSS, all mice had at least two to three macroscopic S1 tumors and at least one S2 or larger tumor when scored by endoscopy (Figure 2A) according to the system by Becker and Neurath (see the STAR Methods) (Becker et al., 2006). Thus, we chose this time point for TAM administration to delete the p53^{floxQ} allele. As controls we used (1) oil-treated p53^{floxQ/-}; ERT2 mice and (2) p53^{-/-}; ERT2 mice treated with oil or TAM.

Indeed, upon TAM-induced mutp53 ablation, tumor multiplicity and size were reduced. Notably, this effect was independent of the presence or absence of a WT p53 allele (Figures 2B and S2A). mutp53 ablation in tumors was validated at the genomic, mRNA, and protein level (Figures 2C, 2D, and S2B–S2E). In p53^{floxQ/+}; ERT2 mice tumor burden decreased from 15 tumors per mouse in oil-treated animals to 9 tumors per mouse in TAM-treated animals (Figure S2A). Likewise, in p53^{floxQ/-}; ERT2

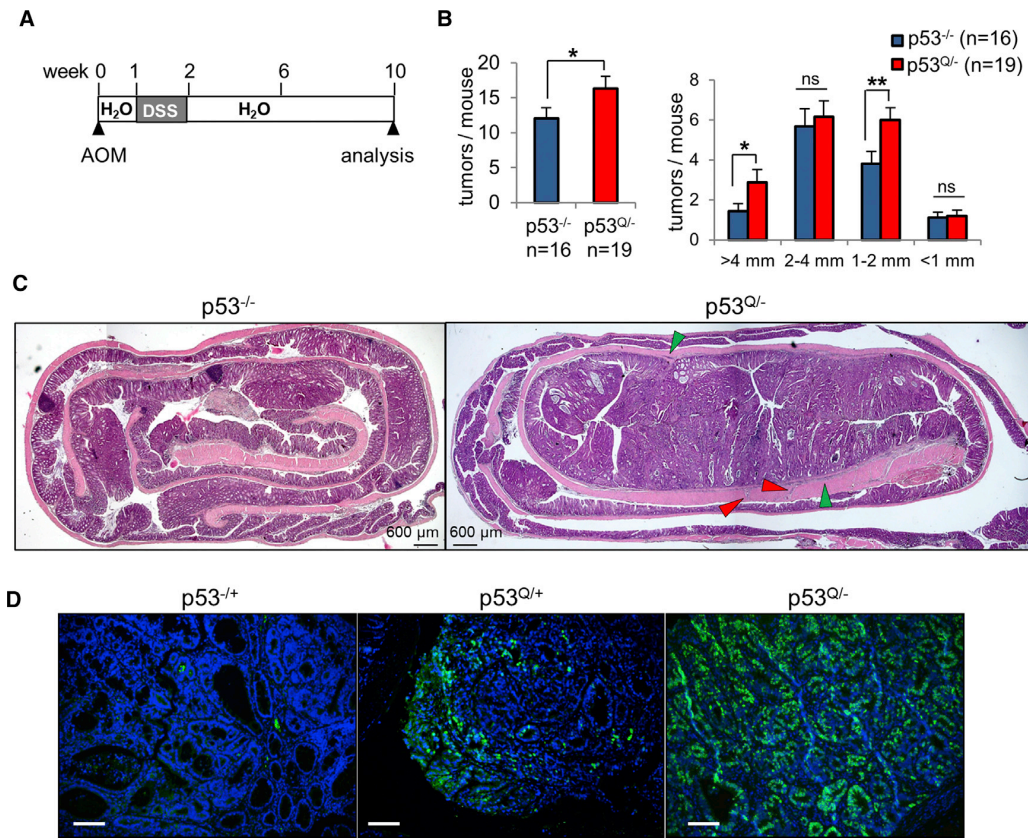


Figure 1. mutp53 Exerts GOF Activity in the AOM/DSS-Induced Mouse Model of Colorectal Cancer

(A) Treatment scheme of the AOM/DSS CRC model. Endpoint at 10 weeks.

(B) Total number of colon tumors per mouse (left) and tumor size distribution (right) of p53^{-/-} and p53^{Q/-} mice at 10 weeks after AOM/DSS. Bars, mean \pm SEM, Student's t test. *p = 0.05; **p = 0.01; ns, not significant.

(C) Colon sections from AOM/DSS-treated p53^{-/-} and p53^{Q/-} mice at endpoint. H&E. Green arrows, invasion into submucosa; red arrows, invasion into muscularis propria.

(D) Representative immunofluorescence staining of p53 (green) in colonic tumor sections from AOM/DSS-treated mice of the indicated genotypes at endpoint 10 weeks (p53^{Q/-}) and 12 weeks (p53^{Q/+} and p53^{-/+}). DAPI counterstain (blue). Scale bars, 100 μ m.

See also Figure S1.

mice, tumor burden decreased from 16 tumors per mouse in oil-treated animals to 11 tumors per mouse in TAM-treated animals (Figure 2B). Moreover, in both mutp53 genotypes, tumor sizes also markedly decreased upon mutp53 ablation (Figures 2B and S2A). In contrast, in both corresponding control groups, TAM treatment had no effect on tumor numbers and sizes (Figures 2B and S2A).

Since the majority of human mutp53 CRC tumors undergo LOH of the WT *TP53* allele (Parikh et al., 2014), we used p53^{flloxQ/-};ERT2 mice to analyze the cellular mechanism of the mutp53 ablation-mediated anti-tumoral response. Apoptosis was not the underlying reason for aborted tumor formation and shrinkage, since no difference was observed between control and ablated tumors for cleaved Casp3 (Figure S2F), or the expression of Noxa and Puma (Figure S2G). We did not observe evidence of necrosis based on histology. The expression level of the CDK inhibitor p16/*Cdkn2A* remained unchanged and that of p21/*Cdkn1A* was undetectable, largely ruling out senes-

cence (Figure S2G). Instead, tumor proliferation was markedly decreased upon mutp53 ablation, indicated by decreased Ki67 staining (Figures 2E and 2F) and PCNA mRNA levels (Figure 2G) in TAM-treated p53^{flloxQ/-};ERT2 compared with control mice. Ki67 and mutp53 nuclear staining intensities strongly correlated (Figure 2H). Thus, ablation of the hotspot GOF p53^Q allele inhibits tumor proliferation, establishing that colonic tumors depend on continuous expression of stabilized mutp53.

Ablation of mutp53 Strongly Inhibits Tumor Cell Invasion in Colorectal Cancer

The presence of WT p53 is a major barrier for tumor invasiveness in most if not all tumor entities including CRC (Riley et al., 2008; Schwitalla et al., 2013). In agreement, p53^{Q/+} mice, which showed no GOF for tumor numbers (Figure S1F), also failed to develop any invasive tumors at endpoint 12 weeks after AOM/DSS (10 mice with a total of >100 tumors analyzed; data not shown). In sharp contrast, in the absence of WT p53,

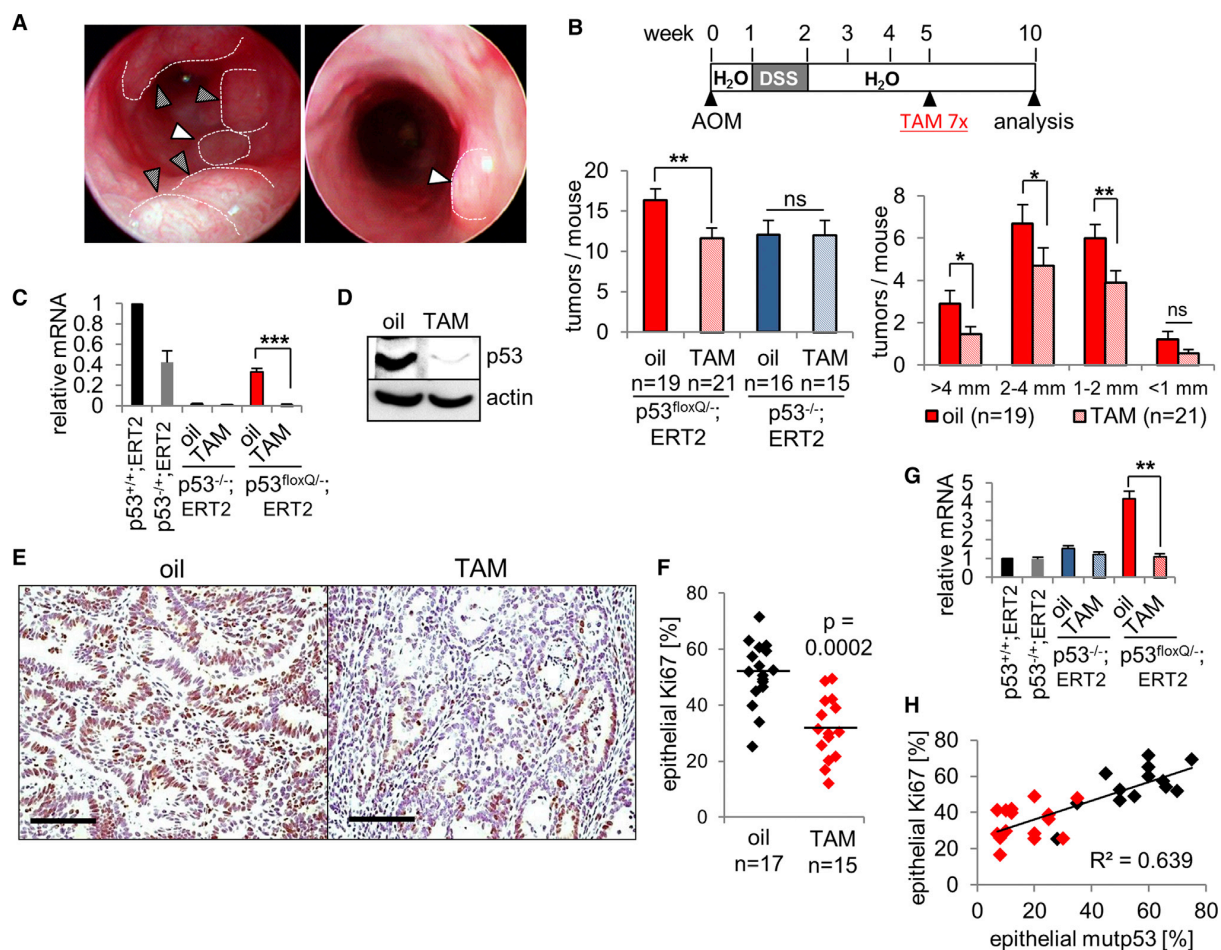


Figure 2. Genetic Ablation of the GOF mutp53 Allele Inhibits Tumor Growth

(A) Colonoscopy images of a $p53^{flloxQ/-};ERT2$ mouse at week 5 after AOM/DSS, exhibiting tumors with scores of S1 (solid arrows) and S2 (dashed arrows) according to Becker and Neurath (Becker et al., 2006). Dotted lines surround tumors.

(B) Schematic presentation of ablating the $p53^{flloxQ}$ allele in mice with AOM/DSS-induced (1.5%) established CRCs (top). Tamoxifen (TAM) or oil treatment was administered at week 5 after AOM, when each mouse had at least two to three S1 tumors and at least one S2 or larger tumor. Tumor numbers per mouse in $p53^{flloxQ/-};ERT2$ and $p53^{-/-};ERT2$ mice and tumor size distribution in $p53^{flloxQ/-};ERT2$ mice at endpoint 10 weeks (bottom). ns, not significant.

(C and D) The p53 mRNA (C) and protein (D) level isolated from colonic tumors from oil- and TAM-treated $p53^{flloxQ/-};ERT2$ mice at 10 weeks after AOM/DSS (pooled samples, $n \geq 5$ tumors per group). Actin, loading control.

(E and F) Standardized Ki67 immunostaining (E) and quantitation of Ki67-positive tumor epithelial cells (F) of $p53^{flloxQ/-};ERT2$ tumors at 10 weeks after AOM/DSS. Scale bars, 100 μm . The quantification was done by counting four random fields (40x) of two tumor sections per mouse. For oil (black) 17 tumors from 6 mice, and for TAM (red) 15 tumors from 5 mice, were counted. Ki67-positive tumor epithelial cells as percentage of total tumor cell nuclei. Black lines, mean. Student's t test.

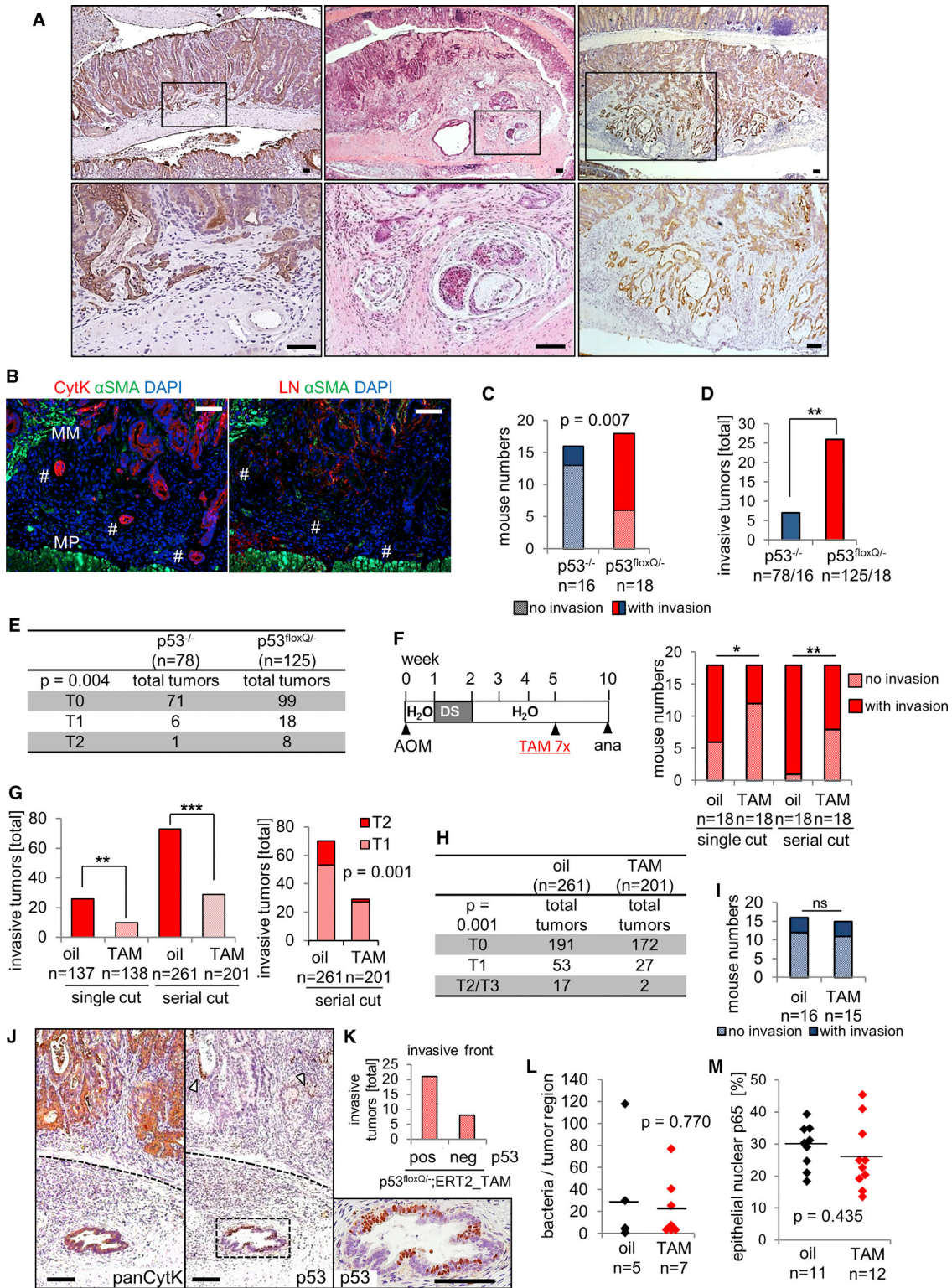
(G) Relative *PcnA* mRNA levels of the indicated groups. qRT-PCR as in (C). (B, C, and G) Bars, mean \pm SEM, Student's t test. * $p = 0.05$; ** $p = 0.01$; *** $p = 0.001$.

(H) Correlation between accumulated nuclear p53 and Ki67 positivity in tumor epithelial cells in $p53^{flloxQ/-};ERT2$ tumors treated with oil (black, $n = 13$ tumors from 6 mice) or TAM (red, $n = 15$ tumors from 6 mice).

See also [Figure S2](#).

mutp53 showed strong GOF for invasiveness at endpoint 10 weeks after AOM/DSS (Figures 3A, 3B, S3A, and S3B). In fact, 12 of 18 (65%) oil-treated $p53^{flloxQ/-};ERT2$ mice harbored one or more invasive tumors, compared with only 3 of 16 (19%) oil-treated $p53^{-/-};ERT2$ control mice (Figure 3C). The number of observed tumors increased from 7 in 16 animals of the control $p53^{-/-};ERT2$ genotype to 26 tumors in 18 $p53^{flloxQ/-};ERT2$ mice, 8 of which were at T2 stage (Figures 3D and 3E).

Importantly, TAM-induced ablation of mutp53 in $p53^{flloxQ/-};ERT2$ mice dramatically inhibited CRC invasiveness compared with oil-treated controls. Specifically, mutp53 removal reduced the percentage of mice with invasive tumors by 55% (Figure 3F). Moreover, when evaluating the total number of invasive tumors per cohort, a 73% reduction in invasiveness and far less tumors at T2 stage were observed (Figures 3G and 3H). In contrast, no reduction in invasiveness by TAM was seen in $p53^{-/-};ERT2$



(legend on next page)

control mice (Figure 3I). These results were independent of the rigor of the histological scoring, i.e., whether each colon roll was analyzed by a single random H&E section (single cut) or by systematic serial sectioning through the entire roll and the more sensitive pan-cytokeratin staining (serial cut) (Figures 3F and 3G). Of note, the comprehensive serial analysis revealed that 95% of oil-treated $p53^{\text{flloxQ}^-}$;ERT2 mice harbored invasive carcinomas (Figure 3F).

The efficiency of Cre recombinase-mediated ablation of alleles *in vivo* is never 100%, potentially setting up a competition between non-recombined and recombined tumor cells (Alexandrova et al., 2015). Thus, we immunostained all $p53^{\text{flloxQ}^-}$;ERT2 tumors from oil- and TAM-treated cohorts for p53 expression at endpoint. Remarkably, while the benign adenomatous tumor bulk of the post-TAM cohort had undergone near complete depletion of mutp53 as expected (Figure S2D), 66% of all post-TAM malignant glands at the front retained their mutp53 expression (Figures 3J and 3K). Thus, the small minority of tumor cells that failed to recombine became enriched at the invasive front, confirming the strong mutp53 GOF for promoting tumor invasion. It is tempting to speculate that, if allele removal with 100% efficiency were possible, suppression of tumor invasion would have been even stronger.

Persistent chronic inflammation is a major promoter of malignancy. Patients with long-standing ulcerative colitis or Crohn's disease have an increased risk of developing colitis-associated CRC (CAC). $p53^{\text{R175H/+}}$ mice were more prone to chronic colitis in DSS-only induced CAC (requiring at least three cycles of DSS) than $p53^{+/+}$ control mice by maintaining persistent nuclear factor κ B (NF- κ B) activation (Cooks et al., 2013). We challenged mice with only one cycle of DSS after AOM, inducing transient colitis. Still, to assess whether the anti-proliferative and anti-invasive effects of mutp53 removal might be due to decreased

inflammation and NF- κ B activation, we analyzed all invasive $p53^{\text{flloxQ}^-}$;ERT2 tumors with or without mutp53 ablation for their inflammation status. Weight loss is a sensitive indicator of persistent inflammation (Bollrath et al., 2009; Cooks et al., 2013). However, except for a brief acute phase during DSS administration, all mice gained similar weight (Figure S3C). While inflammation was present during tumor initiation, thorough histologic analysis at endpoint showed no differences in number of lymphoid aggregates or degree of stromal inflammatory infiltrates between mutp53-containing and ablated colons in both the polypoid tumor masses and invasive fronts (Figures S3D and S3E). Loss of WT p53 in colonic epithelium triggers bacterial tumor infiltration, thus sustaining inflammation and tumor progression (Schwitalla et al., 2013). While we did detect bacterial infiltrates, their extent was unaltered by mutp53 ablation (Figures 3L and S3F), suggesting that mutp53 GOF does not promote bacterial infiltrates beyond the $p53^{-/-}$ level. We also found no evidence for mutp53-dependent activation of NF- κ B signaling, shown to play a major role in isolated AOM- or DSS-only models of CRC (Cooks et al., 2013; Greten et al., 2004). Analysis of nuclear p65 expression in tumors including the invasive front showed no difference in oil- versus TAM-treated mice, neither in tumor epithelial nor in stromal cells (Figures 3M, S3G, and S3H). In agreement, expression of the NF- κ B target gene iNOS (Hatano et al., 2001) was generally low and showed no difference between the oil/TAM groups (Figure S3I).

Broad profiling of the inflammatory proteome of tumor lysates for levels of chemokines, cytokines, inflammation-associated growth factors and their receptors also failed to show differences between mutp53-expressing and ablated tumors. Only 5 of 111 inflammatory regulators showed mild changes (max. 2.0-fold, Figures S3J–S3L). Interestingly, increased levels of these five gene products are found in CRCs, i.e., CXCL1 and CXCL2 (Erreni

Figure 3. Ablation of mutp53 Strongly Inhibits Invasion in Colorectal Cancer

(A) Representative histopathology of $p53^{\text{flloxQ}^-}$;ERT2 colon tumors 10 weeks after AOM/DSS with extensive invasion. Rectangles at the top row indicate enlarged areas shown at the bottom. Left (right), pan-cytokeratin staining; middle, H&E. Scale bars, 100 μ m.

(B) Immunofluorescence staining for α -smooth muscle actin (α -SMA) (smooth muscle marker, green), pan-cytokeratin (CytK) (epithelial marker, red), or Laminin (LN) (basement membrane marker, red), and DAPI (blue). Serial sections of invasive tumors from $p53^{\text{flloxQ}^-}$;ERT2 mice at endpoint. Note that small invasive cell clumps lack basement membrane staining (*). MM, muscularis mucosae; MP, muscularis propria. Scale bars, 100 μ m.

(C and D) Number of mice scoring positive for one or more invasive tumors (C) and total invasive tumor numbers (D) in $p53^{-/-}$;ERT2 and $p53^{\text{flloxQ}^-}$;ERT2 mice at 10 weeks after AOM/DSS. (C) Fisher's exact test. n = number of mice. (D) n = 78 and 125 tumors from 16 to 18 mice, respectively. Fisher's exact test compared with non-invasive tumors, see also (E).

(E) Quantitation of invasive stages (T0, T1, and T2) from (D). n = total tumors per group. Analysis based on scoring a single random H&E section per colon roll. Chi-square test.

(F and G) Number of mice with invasive tumors (F) and total tumor numbers (G) without (left) or with (right) tumor stage per cohort of $p53^{\text{flloxQ}^-}$;ERT2 mice without or with mutp53 ablation at endpoint 10 weeks. "Single cut," based on scoring a single random H&E section per colon roll. "Serial cut," based on scoring the entire roll by serial sectioning. (F) n = number of mice. (G) n = total tumors. Fisher's exact test compared with non-invasive tumors (right), or to indicated groups (left).

(D, F and G) *p = 0.05; **p = 0.01; ***p = 0.001.

(H) Quantitation of invasive stages (T0, T1, and T2/T3) of serially cut tumors from (G). n = total tumors per group. Note, T3 stage tumors only occur within the oil group with n = 2. Chi-square test.

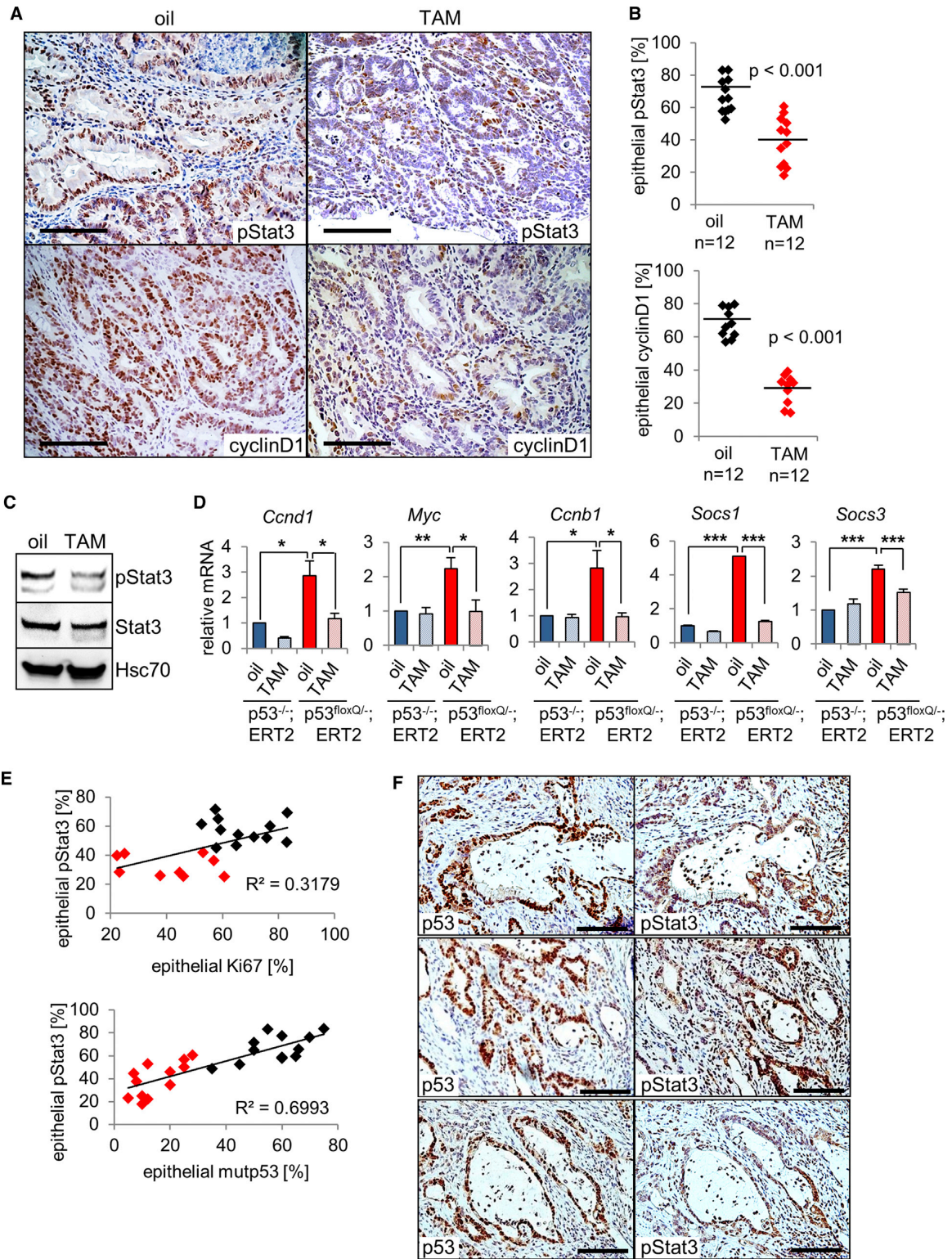
(I) Control $p53^{-/-}$;ERT2 group at 10 weeks after AOM/DSS, assessed for invasiveness as in (C). n = number of mice analyzed. ns, not significant.

(J and K) Example of an invasive gland at the front within the muscularis propria with mutp53 stabilization (J) and quantitation of p53 retention (K) of all invasive tumor fronts of $p53^{\text{flloxQ}^-}$;ERT2 mice that had been TAM treated at 5 weeks after AOM/DSS and analyzed at endpoint 10 weeks. Dashed line, border between submucosa and muscularis propria. Arrowhead, remaining p53. Scale bars, 100 μ m.

(L) Bacterial counts per tumor region from fluorescence *in situ* hybridization analysis of tumors at 10 weeks after AOM/DSS with a Cy5-labeled universal eubacterial probe (EUB 338). At least four random images per tumor were counted. n = 5 tumors from 5 mice for the oil group, and n = 7 tumors from 7 mice for the TAM group.

(M) Quantitation of NF- κ B p65-positive tumor nuclei as percentage of total tumor nuclei at 10 weeks after AOM/DSS. Four random fields (40 \times) of two standardized NF- κ B p65-immunostained tumor sections per colon were counted. For oil (black) 11 tumors from 4 mice and for TAM (red) 12 tumors from 5 mice were counted. Student's t test. (L and M) Black lines, mean.

See also Figure S3.



(legend on next page)

et al., 2009), CHI3L1 (Chen et al., 2011), OPN/Osteopontin (Mole et al., 2011), and OSF2/Periostin (Ben et al., 2009), and all are downregulated upon mutp53 ablation. The chemokines CXCL1 and CXCL2 can attract neutrophils, and their receptor CXCR2 is required for inflammation-driven tumorigenesis (Jamieson et al., 2012). In agreement, the number of tumor-infiltrating neutrophils decreased upon mutp53 ablation (Figures S3M and S3N). In sum, we found that major characteristics of chronic, tumor-promoting inflammation do not depend on the presence of mutp53 compared with the p53^{-/-} situation. Neither lymphocyte abundance, NF- κ B signaling, nor bacterial infiltration are dependent on mutp53. However, more subtle differences such as chemokine secretion and neutrophil attraction might be modulated by mutp53 as part of its GOF.

The Anti-proliferative and Anti-invasive Effects of mutp53 Ablation Are Linked to Suppression of Stat3 Signaling in Tumor Epithelial Cells

We searched for an alternative molecular mechanism to explain both the mutp53-mediated GOF and the mutp53 ablation-mediated anti-tumoral effects. In pancreatic cancer cells, loss of WT p53 activates the Jak2-Stat3 signaling pathway (Wormann et al., 2016). Stat3 signaling, in turn, is a major player in CRC progression (Lin et al., 2011). Indeed, when comparing CRCs of p53^{flloxQ/-};ERT2 with those of p53^{+/+} or p53^{-/-} mice, we found markedly increased levels of pTyr705-Stat3, affecting 100% of p53^{flloxQ/-};ERT2 mice (Figures S4A and S4B), indicating hyperactivation of Stat3 by mutp53, independent of WTp53 loss. Even more importantly, TAM-mediated mutp53 ablation caused a marked reduction of pStat3 in tumors (Figures 4A and 4B). In contrast, stromal Stat3 activity was unchanged (Figure S4C). Immunoblot analysis of tumor extracts confirmed that pStat3 is downregulated (Figure 4C). Stat3 activation drives cell-cycle progression during colitis-associated CRC by inducing the expression of *Ccnd1*, *Myc*, and *Ccnb1* (among other genes) (Bollrath et al., 2009). In support, we found these factors reduced in response to mutp53 ablation (Figures 4A, 4B, and 4D). Expression of the Stat3 target genes *Socs1* and *Socs3* (Hu et al., 2015) was also downregulated after mutp53 ablation (Figure 4D). Quantitative immunohistochemical analysis (IHC) of the tumor epithelial compartment of oil- and TAM-treated p53^{flloxQ/-};ERT2 tumors confirmed correlations between proliferation (Ki67) and pStat3, and between mutp53 and pStat3, including malignant glands at the invasive front (Figures 4E and 4F).

In sum, loss of mutp53 consistently decreased pStat3 signaling in CRC cells. Of note, this was observed on a p53-null background. Thus, despite the known ability of WT p53 to suppress Stat3 activity (Lin et al., 2002; Wormann et al., 2016), the mutp53 GOF of activating Stat3 occurs independent of WT p53 loss.

mutp53 Activates Stat3 Phosphorylation in Human CRC Cells, Resulting in Epithelial-to-Mesenchymal Transition and Cell Migration

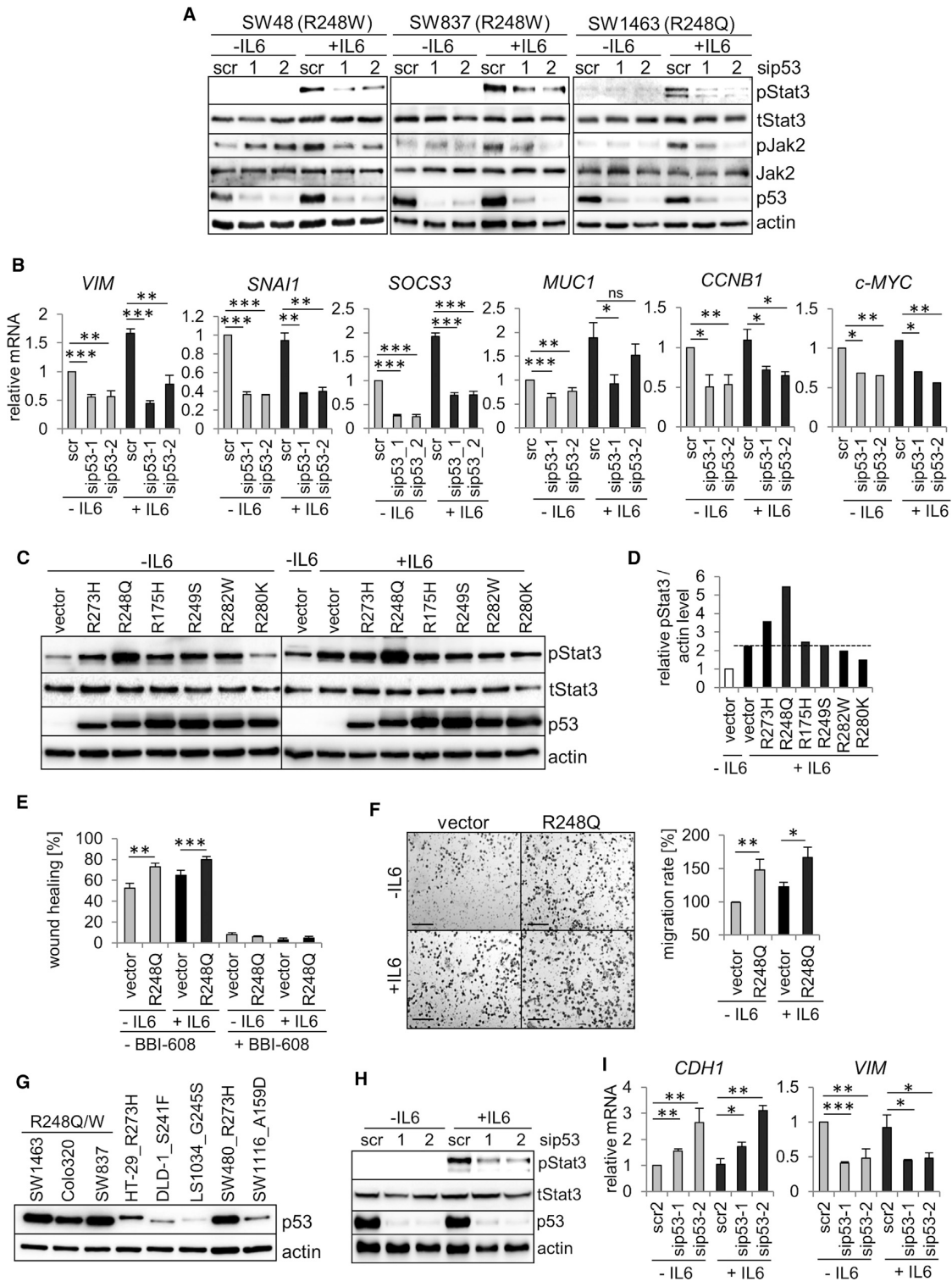
Since mutp53 GOF hyperactivated Stat3 exclusively in tumor but not stromal cells in our mouse model (Figures 4A–4F and S4C), we attempted to recapitulate this phenomenon in human CRC cell lines harboring p53 R248Q/W mutations (SW48, SW837, and SW1463). Indeed, knockdown of mutp53 in these cells by small interfering RNA (siRNA) markedly suppressed interleukin-6 (IL-6)-induced pStat3 (Figure 5A), confirming the mouse model results. The major upstream kinase of Stat3, Jak2, also displayed reduced phosphorylation at Y1007/1008 (Figure 5A). Furthermore, depleting p53 from R248Q/W-containing CRC cell lines greatly blunted IL-6-induced changes in Stat3 target gene expression driving epithelial-to-mesenchymal transition (EMT) and cell cycle (Figures 5B, S5A, and S5B). Upon expression of various p53 hotspot missense mutants in *TP53*^{-/-} H1299 and HCT116 cells, some p53 mutants augmented Stat3 phosphorylation. The R248Q mutant was particularly active in this regard, while other mutants showed a lower ability to do so (Figures 5C, 5D, and S5C–S5E).

To clarify whether mutp53 induces migration and invasion through enhancing Stat3 phosphorylation, we used the Jak2 inhibitor Ruxolitinib and the Stat3 inhibitor BBI-608, which completely block R248Q-mediated Stat3 activation (Figures S5F–S5H). Indeed, wound healing and transwell assays confirmed that R248Q expression greatly increases cell migration in a pStat3-dependent manner, since it was completely blocked by Stat3 inhibition (Figures 5E, 5F, and S5I–S5K).

Next, we sought to determine why p53 R248 mutants show particularly strong pStat3 activation. In a panel of human CRC cell lines with different p53 mutations, all p53 R248Q/W-containing cells showed high steady-state levels of mutp53, whereas most other p53 mutants accumulated to a lesser degree (Figure 5G). Interestingly, SW480 cells (p53 R273H) also expressed high levels of mutp53, while knockdown of mutant p53 again reduced their pStat3 level and modulated their EMT gene

Figure 4. The Anti-proliferative and Anti-invasive Effects of mutp53 Ablation Are Linked to Suppression of Stat3 Signaling in Tumor Epithelial Cells

- (A) Representative examples of immunostaining of p53^{flloxQ/-};ERT2 tumors for pTyr705-Stat3 (pStat3) and cyclin D1 at endpoint 10 weeks after AOM/DSS. Scale bars, 100 μ m.
- (B) Quantitation of (A) as in Figure 2F. pStat3- and cyclin D1-positive tumor epithelial nuclei as percentage of total tumor cell nuclei. For oil (black) 12 tumors from 6 mice and for TAM (red) 12 tumors from 6 mice were counted. Black lines, mean. Student's t test.
- (C) Immunoblot of pStat3 and total Stat3 in tumors from p53^{flloxQ/-};ERT2 mice (pooled samples, n \geq 5 tumors per group) at 10 weeks after AOM/DSS. Hsc70, loading control.
- (D) qRT-PCR analysis of mRNA levels of the indicated Stat3 target genes isolated from tumors at 10 weeks after AOM/DSS and normalized to 36B4 mRNA. n \geq 5 tumors per group. Mean \pm SEM of three to five technical replicates, in triplicates. Student's t test. *p = 0.05; **p = 0.01; ***p = 0.001.
- (E) Correlations in quantitative immunostaining as in (A and B) between pStat3 and Ki67 and between pStat3 and mutp53 in epithelial cells of p53^{flloxQ/-};ERT2 tumors treated with oil (black) or TAM (red). Top, oil n = 12 tumors from 6 mice; TAM n = 9 tumors from 5 mice. Bottom, oil n = 12 tumors from 6 mice; TAM n = 12 tumors from 6 mice. R, Pearson correlation factor.
- (F) Representative p53 and pStat3 staining in colonic tumors of an oil-treated p53^{flloxQ/-};ERT2 mouse at 10 weeks after AOM/DSS. Scale bars, 100 μ m. See also Figure S4.



(legend on next page)

expression (Figures 5H and 5I). In contrast, CRC cell lines with low levels of mutp53 did not alter their pStat3 levels upon p53 depletion (Figures 5G and S5L), pointing to a preferential ability of p53 mutants with high steady-state levels to hyperactivate Stat3.

Highly Stabilized mutp53 Constitutively Activates Stat3 Phosphorylation by Physical Interaction with pStat3, Protecting It from Dephosphorylation by SHP2 Phosphatase

Next we asked why the p53 R248Q mutant showed particularly high levels. Interestingly, the differences in p53 levels consist at least in part in half-life differences of the various mutants, as revealed by cycloheximide chase experiments (Figure S6A) and by comparative expression of p53 hotspot mutants in *TP53*^{-/-} HCT116 cells (Figures S6B and S6C).

Mechanistically, the activation of Stat3 by mutp53 is based on physical interaction. Co-immunoprecipitation revealed that both the R248Q and R248W mutants interacted with the endogenous total Stat3 and pStat3 in CRC cells (Figure 6A). Moreover, ectopic p53 hotspot mutants including R248Q also formed complexes with endogenous Stat3 in *TP53*^{-/-} cells (Figures 6B and 6C). Notably, the ability of mutp53 to bind to Stat3 correlates with the degree of its stabilization (Figures 5G, 6C, and 6D).

Next we asked how this interaction affects Stat3 phosphorylation. Strikingly, modulation of mutp53 levels revealed that mutp53 disrupts the association between Stat3 and its robust negative regulator the tyrosine phosphatase SHP2, thereby protecting pStat3 from dephosphorylation (Figures 6E–6G). PTPN11/SHP2 is a tumor suppressor in liver cancer and CRC (Bard-Chapeau et al., 2011; Huang et al., 2017), and, indeed, SHP2 depletion increased Stat3 phosphorylation in CRC cells (Figure 6E). Importantly, p53 R248Q expression destroyed pStat3-SHP2 complexes while increasing the amount of mutp53-pStat3 complexes (Figure 6F). Conversely, depletion of endogenous p53 R248Q/W in CRC cells greatly enhanced binding of SHP2 to Stat3 (Figure 6G, seen by the newly detectable band labeled #).

Thus, p53 R248Q hyperactivates Stat3 by competitive displacement of SHP2, the tyrosine phosphatase for Stat3. The

physical interaction between stabilized abundant mutp53 and pStat3 prevents pStat3 from associating with its phosphatase. pStat3 is protected from dephosphorylation and remains active.

mutp53 Expression Correlates with Jak2/Stat3 Activation and Poor Survival in CRC Patients

Quantitative standardized IHC analysis of human primary CRC (n = 98 cases, Figure S7A) showed a correlation between stabilized nuclear mutp53 (p53^{high}, a surrogate marker for p53 missense mutations) and high levels of activated pJak2 (Figures 7A and 7B) and pStat3 (Figures 7A and 7C). In CRC the main pathway of Stat3 activation is via Jak2 (Figure S7B). Moreover, both parameters combined or in isolation were associated with shorter patient survival, i.e., patients with pJak2^{high}/p53^{high} had a median survival of 45 versus 76 months in patients with pJak2^{low}/p53^{low} (Figures 7D and S7C), and patients with pStat3^{high}/p53^{high} had a median survival of 48 versus 68 months in patients with pStat3^{low}/p53^{low} (Figure 7E). Importantly, pJak2^{high}/p53^{high} or pStat3^{high}/p53^{high}, or p53^{high} alone, was also associated with higher numbers of lymph nodes with metastases (Figures 7F, 7G, and S7D), confirming a pro-invasive role for mutp53 in human CRC. In further support of the p53/pStat3 interaction, both proteins co-localize in CRC tumor nuclei (Figure S7E). Notably, p53 mutational analysis of all subgroups in Figure 7C confirmed the p53/pStat3 staining correlations (Figures S7F–S7H). As important independent confirmation, analysis of all publically available reverse-phase protein array datasets from an unrelated human CRC cohort again revealed that R248 missense mutant tumors express higher pTyr705-Stat3 levels than all other missense or nonsense mutant or WT *TP53* CRCs (Figure 7H).

When all publically available International Cancer Genome Consortium (ICGC) tumor data were analyzed, patients with tumors harboring p53 R248Q/W mutations exhibited poorer survival than patients with all other nonR248 missense mutations, both within individual tumor types (Figures 7I, 7J, and S7I) and across all types (Figure S7I). While this could not be tested for CRC due to insufficient patient samples with annotated clinical data, poorer survival was seen in other p53 R248Q/W gastrointestinal cancers and in head and neck cancers (Figures 7J and

Figure 5. mutp53 Activates Stat3 Phosphorylation in Human CRC Cells, Resulting in EMT and Cell Migration

(A) In human CRC cell lines carrying R248 missense mutations, after knockdown of mutp53 by siRNA, pStat3 and pJak2 levels were determined. At 48 hr after transfection with two different p53 siRNAs or scrambled (scr) control siRNAs, cells were treated with IL-6 or left untreated for 24 hr. Immunoblot analysis. tStat3, total Stat3.

(B) qRT-PCR analysis of the relative mRNA levels of indicated Stat3 target gene expression in SW1463 cells. At 24 hr after transfection with two siRNAs targeting mutp53, cells were treated +/- IL-6 for 72 hr and then harvested for RNA isolation. Mean ± SEM of two independent experiments, each repeated twice in triplicate, Student's t test. ns, not significant.

(C) p53 hotspot mutants were expressed in H1299 cells (*TP53*^{-/-}) to analyze their impact on Stat3 phosphorylation. At 48 hr after transfection with expression plasmids, cells were +/- IL-6-treated for 24 hr, followed by immunoblot to detect pStat3.

(D) Densitometry of immunoblot in (C), right part. Dashed line, level of activated pStat3 with IL-6 only.

(E) Wound healing as assessed by scratch assay. H1299 cells were transfected with plasmids to express p53 R248Q or empty backbone and treated +/- IL-6 and +/- Stat3 inhibitor BBI-608 (500 nM). Wound healing was assessed after 24 hr.

(F) Representative images (left) and quantification (right) of transwell migration assay of H1299 cells expressing p53 R248Q treated +/- IL-6. (E and F) Mean ± SEM of two independent experiments in duplicates, Student's t test. Scale bars, 200 μm.

(G) Immunoblot analysis comparing the endogenous mutp53 levels of the indicated CRC cell lines.

(H) The impact of mutp53 on pStat3 levels was assessed by knockdown of mutp53 by two different siRNAs in SW480 (*TP53*^{R273H}) cells as in (A), followed by immunoblot analysis of pStat3.

(I) EMT marker expression in SW480 cells upon mutp53 depletion as in (B). Mean ± SEM, Student's t test.

*p = 0.05; **p = 0.01; ***p = 0.001. Actin is used as a loading control in (A, C, G, and H). See also Figure S5.

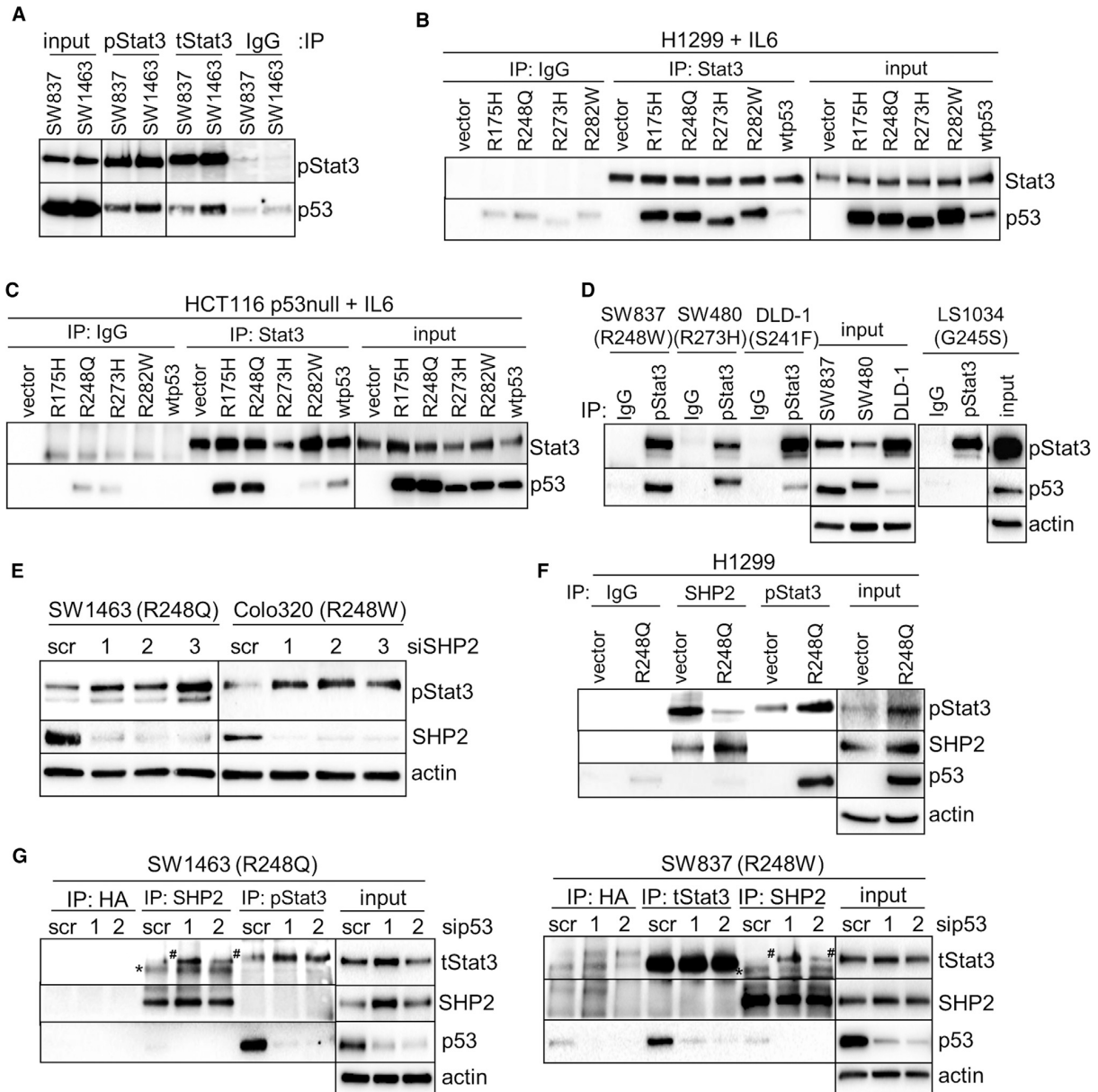
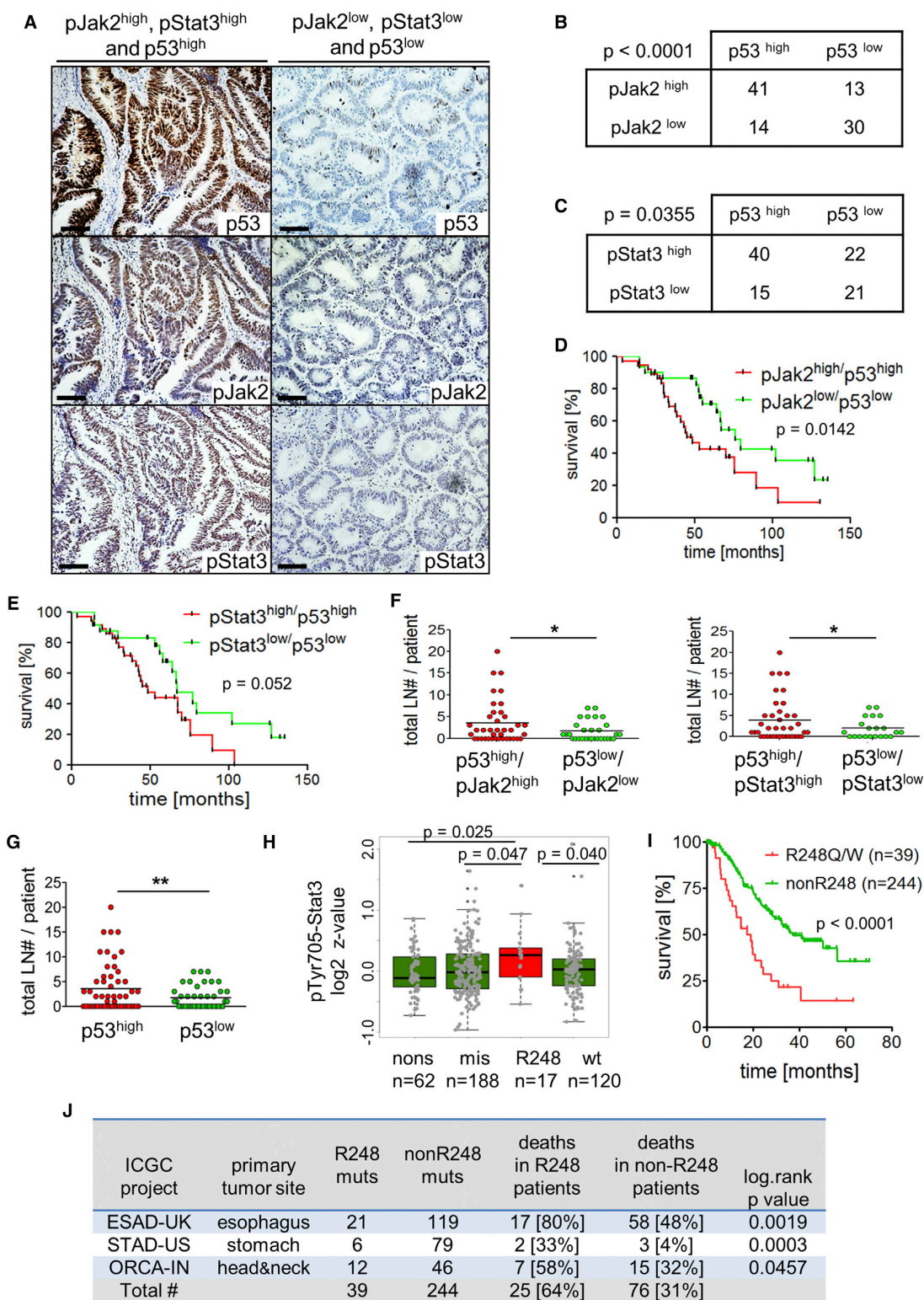


Figure 6. Highly Stabilized mutp53 Binds and Constitutively Activates Stat3 Phosphorylation, Displacing SHP2 Phosphatase
 (A) Untreated SW837 and SW1463 cells were subjected to co-immunoprecipitation (coIP) with anti-pTyr705-Stat3, anti-tStat3, or immunoglobulin G (IgG) antibodies, followed by immunoblot.
 (B and C) *TP53*^{-/-} H1299 (B) and HCT116 (C) cells were transfected with p53 expression plasmids, and then treated with IL-6 and subjected to coIP with Stat3 and IgG antibodies, followed by immunoblot.
 (D) IL-6-treated cells were subjected to coIP as in (A).
 (E) pStat3 levels were analyzed by immunoblot in response to SHP2 knockdown in human CRC cells. At 48 hr post transfection with three different SHP2 siRNAs or scr control siRNA, cells were treated with IL-6 for 24 hr.
 (F) The impact of mutp53 R248Q on pStat3-SHP2 and pStat3-mutp53 complexes. H1299 cells were transfected with expression plasmids for mutp53 R248Q or empty vector and 48 hr later subjected to coIP with anti-SHP2, anti-pTyr705-Stat3, or IgG antibodies as in (A), followed by immunoblot.
 (G) Upon depletion of endogenous mutp53 R248Q/W in CRC cells, the binding of SHP2 to Stat3 was assessed. At 48 hr after transfection with siRNAs, cells were treated with IL-6 for 24 hr and subjected to coIP followed by immunoblot as in (A). # specific band, *non-specific band.
 (A–D, F, and G) Input, 5% of coIP. See also Figure S6.



(legend on next page)

S7I). Moreover, a higher death risk was even present when all available 21 cancer types of the ICGC datasets were analyzed in aggregate, which includes many entities with only a single or few R248Q/W cases (Figure S7I).

Overall, these patient data confirm the strong GOF activity of the high steady-state mutant R248Q/W whose molecular mechanism in CRC operates in part by dysregulating the Jak2/Stat3 pathway, and, importantly, creates tumor vulnerabilities that might be therapeutically exploitable.

Pharmacological Inhibition of Hsp90 Reduces mutp53 Levels and Inhibits Initiation and Progression of Mouse CRCs

The constitutive stabilization of mutp53 in tumors is a key feature and prerequisite of GOF (Alexandrova et al., 2015). The HSP90 chaperone system that is ubiquitously activated in cancer is a major determinant of mutp53 stabilization by blocking its degradation. For spontaneously arising T cell lymphomas in GOF mutp53 knockin mice (p53^{Q/-} and p53^{H/H}), we previously showed that Hsp90 inhibitors are capable of reducing mutp53 levels and triggering strong anti-tumoral responses *in vivo*. This translates to major gains in survival specifically in GOF mutp53 mice, but not in their p53^{-/-} littermates, even in the absence of WT p53 (Alexandrova et al., 2015; Li et al., 2011b). This prompted us to test whether Hsp90 inhibition will also overcome the impact of mutp53 GOF in CRC progression. Indeed, p53^{Q/-} mice induced with AOM/DSS developed CRCs to a far lesser extent when treated with the Hsp90 inhibitor 17AAG compared with vehicle controls (Figures 8A–8E). Four weeks of treatment of mice bearing later-stage S3 CRCs achieved clear tumor inhibition (Figures 8A and 8B). This therapeutic effect was even more pronounced when 17AAG was started at earlier tumor stages when it apparently prevented tumor onset (Figures 8C and 8D). Concomitantly, Hsp90 inhibition profoundly reduced mutp53 levels in tumors (Figures 8F, S8A, and S8B), while apoptotic marker-cleaved caspase-3 and DNA-damage marker γ H2AX were greatly upregulated (Figure 8G). Importantly, pStat3 levels were also reduced after Hsp90 inhibition (Figures 8H and S8C). In p53^{-/-} control mice this effect was much less pronounced than in p53^{Q/-} mice, although 17AAG showed a weak trend to reduced tumor size

(Figure S8D), which is not surprising given the plethora of HSP90 client proteins (Schopf et al., 2017).

In sum, these data indicate that mutp53 degradation is a major mechanism in the therapeutic impact of Hsp90 inhibition on CRC growth. Thus, mutp53 not only is a critical driver in CRC progression, but an actionable target that is druggable by HSP90 inhibition, leading to an effective anti-tumor response *in vivo*.

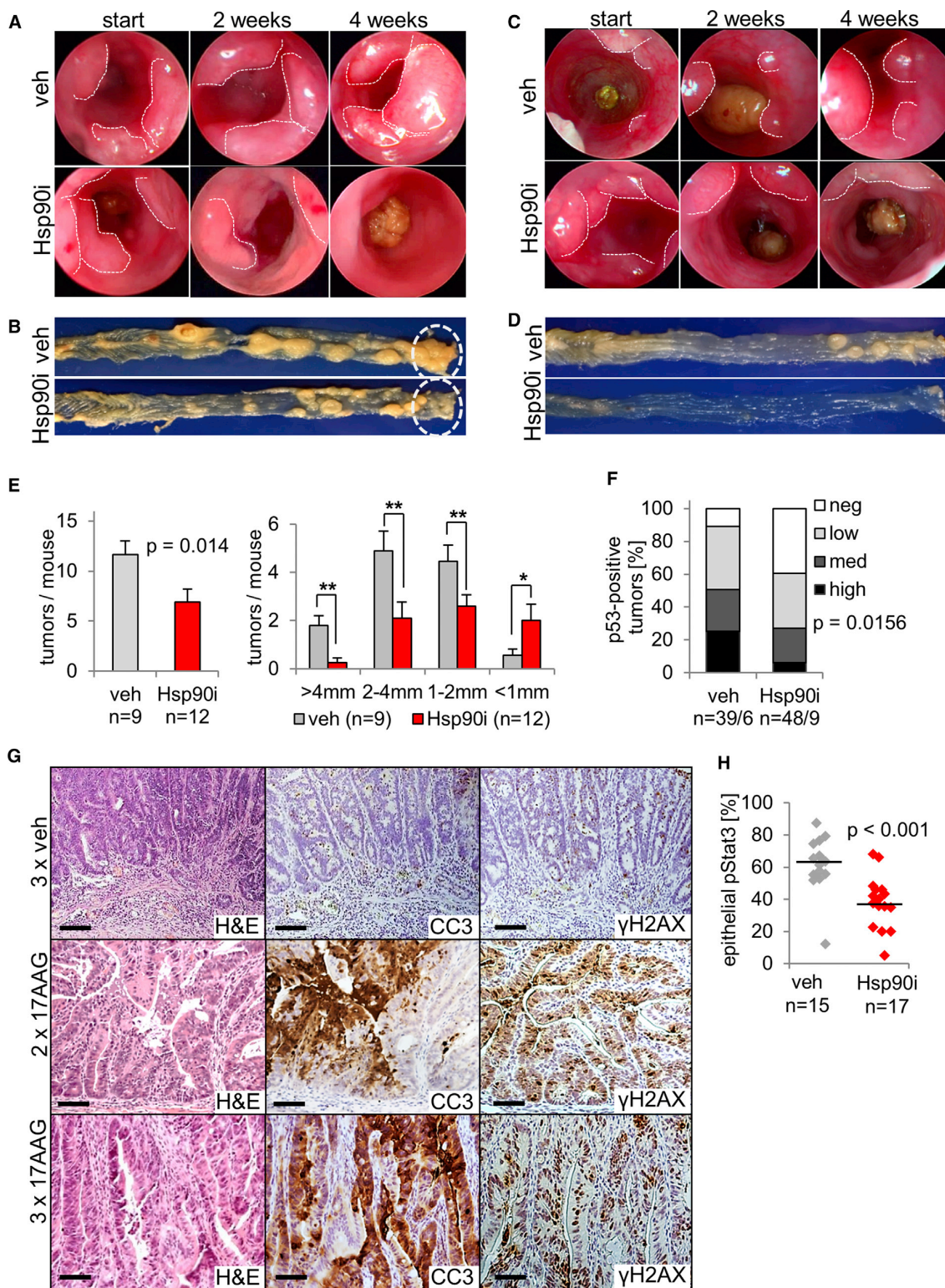
DISCUSSION

Here we used an autochthonous immune-competent mouse model that faithfully recapitulates molecular mechanism, pathology, and progression of human CRC to determine the biological importance of the single most common mutant p53, R248Q, in CRC development and as potential drug target. We show that this tumor entity is driven by the GOF activity of this mutp53 allele. Compared with p53^{-/-} tumors, stabilized mutp53 R248Q protein enhances size, multiplicity, and invasiveness of colonic tumors by constitutive hyperactivation of Jak2/Stat3 signaling. Strikingly, this mutp53 dependency creates tumor-specific vulnerabilities that can be exploited therapeutically. Genetic removal of mutp53 in established CRC strongly reduces all these parameters, establishing tumor dependence on continuously elevated mutp53 levels. Likewise, pharmacological degradation of mutp53 by an HSP90 inhibitor markedly antagonizes CRC. Importantly, CRC patients with accumulated mutp53 also exhibit enhanced Jak2/Stat3 signaling and poorer survival. In sum, our data endorse mutp53, in particular (but not exclusively) when carrying R248 mutations, as molecular target in CRC therapy.

The p53^{Q/-} genotype model we studied here reflects a common human p53 tumor genotype. In a meta-analysis across multiple cancer types (2,256 tumors of 10 common cancers including 157 CRC cases), 21% of all tumors and 30% of CRCs were of the missense mutp53/p53del genotype (Parikh et al., 2014). Strikingly, we find that the poorest patient survival associates specifically with p53 R248Q/W mutations versus all nonR248 mutations across all tumor types, expanding an earlier Cancer Genome Atlas (TCGA) analysis (Xu et al., 2014). This strongly suggests that R248 missense alleles confer a specific clinically relevant GOF. Importantly, the R248 hotspot is the

Figure 7. mutp53 Expression Correlates with Stat3 Activation and Poor Survival in CRC Patients

(A) Serial sections of two representative human CRC tumors immunostained for p53, pJak2, and pStat3. Scale bars, 100 μ m.
 (B and C) Correlation between stabilized mutp53 (p53^{high}) and pJak2 (B) or pStat3 (C) in primary human colorectal carcinomas. n = 98 cases, Fisher's exact test.
 (D and E) Median survival of CRC patients with p53^{high}/pJak2^{high} tumors (45 months) versus those with p53^{low}/pJak2^{low} tumors (76 months) (D), and CRC patients with p53^{high}/Stat3^{high} tumors (48 months) versus those with p53^{low}/pStat3^{low} tumors (68 months) (E). Kaplan-Meier statistic on cohorts from (B and C), log-rank tests.
 (F) Number of lymph nodes (LN) with metastases in CRC patients stratified by p53^{high}/pJak2^{high} tumors (n = 40, mean 3.5 positive LN) versus p53^{low}/pJak2^{low} tumors (n = 30, mean 1.6 positive LN) or by p53^{high}/pStat3^{high} tumors (n = 39, mean 3.9 positive LN) versus p53^{low}/pStat3^{low} tumors (n = 21, mean 1.9 positive LN).
 (G) Similar to (F) but patients were stratified by p53^{high} tumors (n = 54, mean 4.1 LN) versus p53^{low} tumors (n = 43, mean 1.7 LN). (F and G) Black lines, mean. (F and G) *p = 0.05; **p = 0.01.
 (H) The pTyr705-Stat3 level is plotted for p53 status using reverse-phase protein array datasets from an unrelated human CRC cohort. Boxplot and whisker plot was made by R with default settings. Box boundary is the first and third quartiles with median line inside. Whiskers were 1.5 interquartile range extended from boundaries.
 (I and J) Kaplan-Meier statistic on patient cohorts from the International Cancer Genome Consortium (ICGC). Patients with cancers harboring TP53^{R248Q/W} missense mutations were compared with patients carrying all (other) nonR248 missense mutations. Three cancer types (esophagus, stomach, and head and neck) listed in (J) with a sufficient total number of TP53^{R248} mutations were analyzed in aggregate (I). The median survival of TP53^{R248} patients is 14.8 versus 40.7 months for patients with nonR248 mutations in TP53. Log-rank test, p < 0.0001. (J) Summary of the three ICGC studies used for Kaplan-Meier analysis in (I) (see also their individual analysis in Figure S7I). ICGC dataset, release no. 25.
 See also Figure S7.



(legend on next page)

single most common variant, occurring in 9% of all *TP53*-altered tumors, which translates to ~66,000 newly diagnosed cancer patients in the US per year harboring R248 variants. Also, mutations at R248 (into Q or W) are among the three most frequent *TP53* alterations in human CRC (Cancer Genome Atlas Network, 2012).

We reported previously that p53 R248Q is a driver of T cell lymphoma in mice, and that this lymphoid malignancy depends on its continued accumulation for tumor maintenance and metastasis (Alexandrova et al., 2015), a phenomenon akin to “oncogene addiction.” Our current study indicates that addiction to mutp53 is not limited to hematologic malignancies but extends to a highly prevalent solid cancer type. This generalization is of considerable significance in translational oncology, given that ~90% of human malignancies are carcinomas and ~50% of those harbor p53 missense mutations (Leroy et al., 2013). The absence of WT p53 alone can increase DSS-only induced colonic tumorigenesis but rarely gives rise to invasion (Chang et al., 2007). Moreover, AOM treatment of mice with p53 deletion specifically in intestinal epithelial cells produces a pathology and gene signature resembling invasive human CRC (Schwitalla et al., 2013). Hence, WT p53 is a relevant tumor suppressor in this model.

In contrast, mutp53 promotes invasion, e.g., via constitutive activation of epidermal growth factor receptor/integrin signaling (Muller et al., 2009) and by antagonizing TAp63 (Adorno et al., 2009). Moreover, we show here that stabilized p53 R248Q, and to a lesser extent other mutp53 proteins, exert GOF by another efficient mechanism. They constitutively deregulate Jak2/Stat3 signaling through physical interaction with pStat3 and competitive displacement of its phosphatase SHP2, a negative regulator of Stat3, within the malignant epithelial compartment to promote growth and invasion. SHP2 is known to inhibit CRC cell proliferation via Stat3 dephosphorylation *in vitro*, and high SHP2 levels in tumors correlate with longer patient survival (Huang et al., 2017). Stat3 is a well-characterized driver of colon cancer and other solid tumors (Yu et al., 2014), promoting cell-cycle progression, invasion, EMT (Rokavec et al., 2014), and survival of human CRC-initiating cells (Lin et al., 2011). The best-characterized pathway to induce Stat3 activity involves IL-6 and Jak2 kinase, and this pathway is required for the development of colitis-associated carcinoma in mouse models (Bollrath et al., 2009; Grivennikov et al., 2009). Thus, hyperactivation of Jak2/Stat3 by mutp53 constitutes a broad-ranging mechanism to fuel CRC progression.

Of note, low level Stat3 activation already occurs by the mere absence of WT p53. Since WT p53 suppresses Stat3 (Lin et al., 2002), its loss activates Stat3 (Spehlmann et al., 2013; Wormann et al., 2016). Stat3 mediates repression of miR-34, thereby promoting EMT, which is antagonized by WT p53. Importantly, our results show that the p53^Q allele strongly increases Stat3 activation over and above the level of WT p53 loss, further driving tumor progression and invasion. Thus, Stat3-driven cancers represent an example where loss of function of WT p53 and the (simultaneous) GOF by mutp53 each contribute to the robust constitutive hyperactivation of the same oncogenic pathway, albeit at different magnitudes.

In conclusion, the strong oncogenic GOF activities of p53 R248Q/W alleles directly contribute to the progression of a significant subgroup of colon cancer patients. The therapeutic impact of depleting mutp53 from established CRCs, even in the absence of WT p53, identifies GOF mutp53 as an actionable target that is druggable by HSP90 inhibition, leading to an effective anti-tumor response *in vivo*.

STAR★METHODS

Detailed methods are provided in the online version of this paper and include the following:

- KEY RESOURCES TABLE
- CONTACT FOR REAGENTS AND RESOURCE SHARING
- EXPERIMENTAL MODELS AND SUBJECT DETAILS
 - Patient Samples
 - Mouse Experiments and Genotyping
 - Cell Culture and Treatment
- METHOD DETAILS
 - CRC Induction, Colonoscopy and Treatment
 - Histological Analysis
 - Plasmids and Reagents
 - Immunoblots, Co-immunoprecipitation (Co-IP), Cytokine Assays
 - Quantitative PCR
 - Scratch Assay
 - Transwell Migration Assay
 - Fluorescent In Situ Hybridization (FISH)
 - Quantitative Immunohistochemistry on Patient Samples
 - RPPA Analysis
 - Survival Analysis of Patient ICGC Data

Figure 8. Pharmacologically Antagonizing Hsp90 Reduces mutp53 Levels and Inhibits CRC Tumors

(A–D) Representative colonoscopy during treatment (A and C) and resected entire colons after 4 weeks of treatment (B and D) of p53^{Q/-} mice treated with vehicle (veh) or Hsp90 inhibitor 17AAG (Hsp90i). Two starting points for treatment were used: “later stage” when each mouse had at least two to three S2 tumors and one S3 tumor (A and B); and “earlier stage” when each mouse had at least two to three S1 tumors and one S2 tumor (C and D). Images of the same colonic region of a given mouse were taken at start, and 2 and 4 weeks later. Dotted lines surround tumors. Circles, distal tumors strongly disappear.

(E) Tumors per mouse and tumor size distribution of p53^{Q/-} mice treated as in (A and C). Early and late treatments were pooled. Mean ± SEM, Student’s t test. *p = 0.05; **p = 0.01; ***p = 0.001.

(F) Quantitation of p53 immunofluorescence staining of p53^{Q/-} tumors from mice in (E). “p53 high,” corresponds to >60% of tumor cells p53-positive; “p53 medium,” to 30%–60%; “p53 low,” to 5%–30%; and “p53 neg,” to <5%. n = 39 and 48 tumors from 6 to 9 mice, respectively. Chi-square test.

(G) Representative H&E and immunostaining for cleaved caspase-3 (CC3) and γ H2AX of p53^{Q/-} tumors treated with vehicle or 17AAG for 2–3 days. Scale bars, 50 μ m.

(H) Quantitation of pStat3-positive tumor nuclei per total tumor nuclei after Hsp90i for 4 weeks. veh, 15 tumors from 5 mice; Hsp90i, 17 tumors from 5 mice. Black lines, mean. Student’s t test.

See also Figure S8.

- QUANTIFICATION AND STATISTICAL ANALYSIS
- DATA AND SOFTWARE AVAILABILITY

SUPPLEMENTAL INFORMATION

Supplemental Information includes eight figures and one table and can be found with this article online at <https://doi.org/10.1016/j.ccell.2018.07.004>.

ACKNOWLEDGMENTS

We thank Yvonne Begus-Nahrmann for her help in establishing endoscopy in mice, Jennifer Appelhans for technical assistance, and Kirsten Reuter-Jessen and Hans-Ulrich Schildhaus for tumor sequencing. U.M.M. is supported by the NIH (2R01CA176647), the Deutsche Forschungsgemeinschaft (MO 1998/2-1), the Wilhelm Sander-Stiftung (2010.085.1), and the Stony Brook Foundation. R.S.-H. is supported by a Dorothea Schlözer Fellowship and the Heidenreich von Siebold program (UMG, Germany). M.D. is supported by the Wilhelm Sander-Stiftung (2016.143.1), German Cancer Aid (70113010) and the Deutsche José Carreras Stiftung (DJCLS R11/14). R.S.-H., L.-C.C., H.B., and M.D. are supported by the Else Kröner-Fresenius-Stiftung (2014_A14). Results shown in Figures 7H–7J and S71–S7L are based on data generated by the TCGA Research Network: <http://cancergenome.nih.gov/>.

AUTHOR CONTRIBUTIONS

Conceptualization, U.M.M. and R.S.-H.; Methodology, R.S.-H., U.M.M., S.J.E., N.S., J.L., and F.G.; Investigation, R.S.-H., S.J.E., N.S., L.-C.C., H.B., and F.C.; Writing – Review & Editing, U.M.M., R.S.-H., and M.D.; Funding Acquisition, U.M.M., R.S.-H., and M.D.; Supervision, U.M.M., R.S.-H., and M.D.

DECLARATION OF INTERESTS

The authors declare no competing interests.

Received: December 4, 2017

Revised: April 27, 2018

Accepted: July 16, 2018

Published: August 13, 2018

REFERENCES

- Adorno, M., Cordenonsi, M., Montagner, M., Dupont, S., Wong, C., Hann, B., Solari, A., Bobisse, S., Rondina, M.B., Guzzardo, V., et al. (2009). A Mutant-p53/Smad complex opposes p63 to empower TGFbeta-induced metastasis. *Cell* 137, 87–98.
- Alexandrova, E.M., Mirza, S.A., Xu, S., Schulz-Heddergott, R., Marchenko, N.D., and Moll, U.M. (2017). p53 loss-of-heterozygosity is a necessary prerequisite for mutant p53 stabilization and gain-of-function in vivo. *Cell Death Dis.* 8, e2661.
- Alexandrova, E.M., Yallowitz, A.R., Li, D., Xu, S., Schulz, R., Proia, D.A., Lozano, G., Dobbstein, M., and Moll, U.M. (2015). Improving survival by exploiting tumour dependence on stabilized mutant p53 for treatment. *Nature* 523, 352–356.
- Bard-Chapeau, E.A., Li, S., Ding, J., Zhang, S.S., Zhu, H.H., Princen, F., Fang, D.D., Han, T., Bailly-Maitre, B., Poli, V., et al. (2011). Ptpn11/Shp2 acts as a tumor suppressor in hepatocellular carcinogenesis. *Cancer Cell* 19, 629–639.
- Becker, C., Fantini, M.C., and Neurath, M.F. (2006). High resolution colonoscopy in live mice. *Nat. Protoc.* 1, 2900–2904.
- Ben, Q.W., Zhao, Z., Ge, S.F., Zhou, J., Yuan, F., and Yuan, Y.Z. (2009). Circulating levels of periostin may help identify patients with more aggressive colorectal cancer. *Int. J. Oncol.* 34, 821–828.
- Blagosklonny, M.V., Toretzky, J., Bohan, S., and Neckers, L. (1996). Mutant conformation of p53 translated in vitro or in vivo requires functional HSP90. *Proc. Natl. Acad. Sci. USA* 93, 8379–8383.
- Bollrath, J., Phesse, T.J., von Burstin, V.A., Putoczki, T., Bennecke, M., Bateman, T., Nebelsiek, T., Lundgren-May, T., Canli, O., Schwitala, S., et al. (2009). gp130-mediated Stat3 activation in enterocytes regulates cell survival and cell-cycle progression during colitis-associated tumorigenesis. *Cancer Cell* 15, 91–102.
- Bunz, F., Dutriaux, A., Lengauer, C., Waldman, T., Zhou, S., Brown, J.P., Sedivy, J.M., Kinzler, K.W., and Vogelstein, B. (1998). Requirement for p53 and p21 to sustain G₂ arrest after DNA damage. *Science* 282, 1497–1501.
- Cancer Genome Atlas Network (2012). Comprehensive molecular characterization of human colon and rectal cancer. *Nature* 487, 330–337.
- Chang, W.C., Coudry, R.A., Clapper, M.L., Zhang, X., Williams, K.L., Spittle, C.S., Li, T., and Cooper, H.S. (2007). Loss of p53 enhances the induction of colitis-associated neoplasia by dextran sulfate sodium. *Carcinogenesis* 28, 2375–2381.
- Chen, C.C., Pekow, J., Llado, V., Kanneganti, M., Lau, C.W., Mizoguchi, A., Mino-Kenudson, M., Bissonnette, M., and Mizoguchi, E. (2011). Chitinase 3-like-1 expression in colonic epithelial cells as a potentially novel marker for colitis-associated neoplasia. *Am. J. Pathol.* 179, 1494–1503.
- Cooks, T., Pateras, I.S., Tarcic, O., Solomon, H., Schetter, A.J., Wilder, S., Lozano, G., Pikarsky, E., Forshew, T., Rosenfeld, N., et al. (2013). Mutant p53 prolongs NF-kappaB activation and promotes chronic inflammation and inflammation-associated colorectal cancer. *Cancer Cell* 23, 634–646.
- De Robertis, M., Massi, E., Poeta, M.L., Carotti, S., Morini, S., Cecchetti, L., Signori, E., and Fazio, V.M. (2011). The AOM/DSS murine model for the study of colon carcinogenesis: from pathways to diagnosis and therapy studies. *J. Carcinog.* 10, 9.
- Erreni, M., Bianchi, P., Laghi, L., Miolo, M., Fabbri, M., Locati, M., Mantovani, A., and Allavena, P. (2009). Expression of chemokines and chemokine receptors in human colon cancer. *Methods Enzymol.* 460, 105–121.
- Fodde, R., Edelmann, W., Yang, K., van Leeuwen, C., Carlson, C., Renault, B., Breukel, C., Alt, E., Lipkin, M., Khan, P.M., et al. (1994). A targeted chain-termination mutation in the mouse Apc gene results in multiple intestinal tumors. *Proc. Natl. Acad. Sci. USA* 91, 8969–8973.
- Fujii, S., Fujimori, T., Kawamata, H., Takeda, J., Kitajima, K., Omotohara, F., Kaihara, T., Kusaka, T., Ichikawa, K., Ohkura, Y., et al. (2004). Development of colonic neoplasia in p53 deficient mice with experimental colitis induced by dextran sulphate sodium. *Gut* 53, 710–716.
- Greten, F.R., Eckmann, L., Greten, T.F., Park, J.M., Li, Z.W., Egan, L.J., Kagnoff, M.F., and Karin, M. (2004). IKKbeta links inflammation and tumorigenesis in a mouse model of colitis-associated cancer. *Cell* 118, 285–296.
- Grivnennikov, S., Karin, E., Terzic, J., Mucida, D., Yu, G.Y., Vallabhapurapu, S., Scheller, J., Rose-John, S., Cheroutre, H., Eckmann, L., and Karin, M. (2009). IL-6 and Stat3 are required for survival of intestinal epithelial cells and development of colitis-associated cancer. *Cancer Cell* 15, 103–113.
- Hanel, W., Marchenko, N., Xu, S., Yu, S.X., Weng, W., and Moll, U. (2013). Two hot spot mutant p53 mouse models display differential gain of function in tumorigenesis. *Cell Death Differ.* 20, 898–909.
- Hatano, E., Bennett, B.L., Manning, A.M., Qian, T., Lemasters, J.J., and Brenner, D.A. (2001). NF-kappaB stimulates inducible nitric oxide synthase to protect mouse hepatocytes from TNF-alpha- and Fas-mediated apoptosis. *Gastroenterology* 120, 1251–1262.
- Hu, T., Yeh, J.E., Pinello, L., Jacob, J., Chakravarthy, S., Yuan, G.C., Chopra, R., and Frank, D.A. (2015). Impact of the N-terminal domain of STAT3 in STAT3-dependent transcriptional activity. *Mol. Cell. Biol.* 35, 3284–3300.
- Huang, Y., Wang, J., Cao, F., Jiang, H., Li, A., Li, J., Qiu, L., Shen, H., Chang, W., Zhou, C., et al. (2017). SHP2 associates with nuclear localization of STAT3: significance in progression and prognosis of colorectal cancer. *Sci. Rep.* 7, 17597.
- Jacks, T., Remington, L., Williams, B.O., Schmitt, E.M., Halachmi, S., Bronson, R.T., and Weinberg, R.A. (1994). Tumor spectrum analysis in p53-mutant mice. *Curr. Biol.* 4, 1–7.
- Jamieson, T., Clarke, M., Steele, C.W., Samuel, M.S., Neumann, J., Jung, A., Huels, D., Olson, M.F., Das, S., Nibbs, R.J., and Sansom, O.J. (2012). Inhibition of CXCR2 profoundly suppresses inflammation-driven and spontaneous tumorigenesis. *J. Clin. Invest.* 122, 3127–3144.

- Kastrinakis, W.V., Ramchurren, N., Rieger, K.M., Hess, D.T., Loda, M., Steele, G., and Summerhayes, I.C. (1995). Increased incidence of p53 mutations is associated with hepatic metastasis in colorectal neoplastic progression. *Oncogene* *11*, 647–652.
- Lang, G.A., Iwakuma, T., Suh, Y.A., Liu, G., Rao, V.A., Parant, J.M., Valentin-Vega, Y.A., Terzian, T., Caldwell, L.C., Strong, L.C., et al. (2004). Gain of function of a p53 hot spot mutation in a mouse model of Li-Fraumeni syndrome. *Cell* *119*, 861–872.
- Leroy, B., Fournier, J.L., Ishioka, C., Monti, P., Inga, A., Fronza, G., and Soussi, T. (2013). The TP53 website: an integrative resource centre for the TP53 mutation database and TP53 mutant analysis. *Nucleic Acids Res.* *41*, D962–D969.
- Levine, A.J., and Oren, M. (2009). The first 30 years of p53: growing ever more complex. *Nat. Rev. Cancer* *9*, 749–758.
- Li, D., Marchenko, N.D., and Moll, U.M. (2011a). SAHA shows preferential cytotoxicity in mutant p53 cancer cells by destabilizing mutant p53 through inhibition of the HDAC6-Hsp90 chaperone axis. *Cell Death Differ.* *18*, 1904–1913.
- Li, D., Marchenko, N.D., Schulz, R., Fischer, V., Velasco-Hernandez, T., Talos, F., and Moll, U.M. (2011b). Functional inactivation of endogenous MDM2 and CHIP by HSP90 causes aberrant stabilization of mutant p53 in human cancer cells. *Mol. Cancer Res.* *9*, 577–588.
- Lin, J., Tang, H., Jin, X., Jia, G., and Hsieh, J.T. (2002). p53 regulates Stat3 phosphorylation and DNA binding activity in human prostate cancer cells expressing constitutively active Stat3. *Oncogene* *21*, 3082–3088.
- Lin, L., Liu, A., Peng, Z., Lin, H.J., Li, P.K., Li, C., and Lin, J. (2011). STAT3 is necessary for proliferation and survival in colon cancer-initiating cells. *Cancer Res.* *71*, 7226–7237.
- Mihara, M., Erster, S., Zaika, A., Petrenko, O., Chittenden, T., Pancoska, P., and Moll, U.M. (2003). p53 has a direct apoptogenic role at the mitochondria. *Mol. Cell* *11*, 577–590.
- Mole, D.J., O'Neill, C., Hamilton, P., Olabi, B., Robinson, V., Williams, L., Diamond, T., El-Tanani, M., and Campbell, F.C. (2011). Expression of osteopontin coregulators in primary colorectal cancer and associated liver metastases. *Br. J. Cancer* *104*, 1007–1012.
- Muller, P.A., Caswell, P.T., Doyle, B., Iwanicki, M.P., Tan, E.H., Karim, S., Lukashchuk, N., Gillespie, D.A., Ludwig, R.L., Gosselin, P., et al. (2009). Mutant p53 drives invasion by promoting integrin recycling. *Cell* *139*, 1327–1341.
- Muller, P.A., and Vousden, K.H. (2014). Mutant p53 in cancer: new functions and therapeutic opportunities. *Cancer Cell* *25*, 304–317.
- Olive, K.P., Tuveson, D.A., Ruhe, Z.C., Yin, B., Willis, N.A., Bronson, R.T., Crowley, D., and Jacks, T. (2004). Mutant p53 gain of function in two mouse models of Li-Fraumeni syndrome. *Cell* *119*, 847–860.
- Parikh, N., Hilsenbeck, S., Creighton, C.J., Dayaram, T., Shuck, R., Shinbrot, E., Xi, L., Gibbs, R.A., Wheeler, D.A., and Donehower, L.A. (2014). Effects of TP53 mutational status on gene expression patterns across 10 human cancer types. *J. Pathol.* *232*, 522–533.
- Riley, T., Sontag, E., Chen, P., and Levine, A. (2008). Transcriptional control of human p53-regulated genes. *Nat. Rev. Mol. Cell Biol.* *9*, 402–412.
- Rokavec, M., Oner, M.G., Li, H., Jackstadt, R., Jiang, L., Lodygin, D., Kaller, M., Horst, D., Ziegler, P.K., Schwitalla, S., et al. (2014). IL-6R/STAT3/miR-34a feedback loop promotes EMT-mediated colorectal cancer invasion and metastasis. *J. Clin. Invest.* *124*, 1853–1867.
- Schopf, F.H., Biebl, M.M., and Buchner, J. (2017). The HSP90 chaperone machinery. *Nat. Rev. Mol. Cell Biol.* *18*, 345–360.
- Schwitalla, S., Ziegler, P.K., Horst, D., Becker, V., Kerle, I., Begus-Nahrmann, Y., Lechel, A., Rudolph, K.L., Langer, R., Slotta-Huspenina, J., et al. (2013). Loss of p53 in enterocytes generates an inflammatory microenvironment enabling invasion and lymph node metastasis of carcinogen-induced colorectal tumors. *Cancer Cell* *23*, 93–106.
- Spehlmann, M.E., Manthey, C.F., Dann, S.M., Hanson, E., Sandhu, S.S., Liu, L.Y., Abdelmalak, F.K., Diamanti, M.A., Retzlaff, K., Scheller, J., et al. (2013). Trp53 deficiency protects against acute intestinal inflammation. *J. Immunol.* *191*, 837–847.
- Tanaka, T., Kohno, H., Suzuki, R., Yamada, Y., Sugie, S., and Mori, H. (2003). A novel inflammation-related mouse colon carcinogenesis model induced by azoxymethane and dextran sodium sulfate. *Cancer Sci.* *94*, 965–973.
- Ventura, A., Kirsch, D.G., McLaughlin, M.E., Tuveson, D.A., Grimm, J., Lintault, L., Newman, J., Reczek, E.E., Weissleder, R., and Jacks, T. (2007). Restoration of p53 function leads to tumor regression in vivo. *Nature* *445*, 661–665.
- Whitesell, L., and Lindquist, S.L. (2005). HSP90 and the chaperoning of cancer. *Nat. Rev. Cancer* *5*, 761–772.
- Whitesell, L., Sutphin, P.D., Pulcini, E.J., Martinez, J.D., and Cook, P.H. (1998). The physical association of multiple molecular chaperone proteins with mutant p53 is altered by geldanamycin, an hsp90-binding agent. *Mol. Cell. Biol.* *18*, 1517–1524.
- Wormann, S.M., Song, L., Ai, J., Diakopoulos, K.N., Kurkowski, M.U., Gorgulu, K., Ruess, D., Campbell, A., Doglioni, C., Jodrell, D., et al. (2016). Loss of P53 function activates JAK2-STAT3 signaling to promote pancreatic tumor growth, stroma modification, and gemcitabine resistance in mice and is associated with patient survival. *Gastroenterology* *151*, 180–193.e12.
- Xu, J., Wang, J., Hu, Y., Qian, J., Xu, B., Chen, H., Zou, W., and Fang, J.Y. (2014). Unequal prognostic potentials of p53 gain-of-function mutations in human cancers associate with drug-metabolizing activity. *Cell Death Dis.* *5*, e1108.
- Yu, H., Lee, H., Herrmann, A., Buettner, R., and Jove, R. (2014). Revisiting STAT3 signalling in cancer: new and unexpected biological functions. *Nat. Rev. Cancer* *14*, 736–746.
- Yue, X., Zhao, Y., Xu, Y., Zheng, M., Feng, Z., and Hu, W. (2017). Mutant p53 in cancer: accumulation, gain-of-function, and therapy. *J. Mol. Biol.* *429*, 1595–1606.

STAR★METHODS

KEY RESOURCES TABLE

REAGENT or RESOURCE	SOURCE	IDENTIFIER
Antibodies		
Rabbit polyclonal anti-Ki67	Abcam	Cat# ab15580; RRID:AB_805388
Rabbit polyclonal anti-p53 (FL-393)	Santa Cruz	Cat# sc-6243; RRID:AB_653753
Rabbit polyclonal anti-wide spectrum cytokeratin	Abcam	Cat# ab9377; RRID:AB_307222
Rabbit polyclonal anti-Laminin	Abcam	Cat# ab11575; RRID:AB_298179
Goat polyclonal anti- α SMA	Abcam	Cat# ab21027; RRID:AB_1951138
Rabbit monoclonal anti-NF- κ B p65 (D14E12) XP	Cell signaling	Cat# 8242; RRID:AB_10859369
Rabbit polyclonal anti-NOS2 (iNOS) (H-174)	Santa Cruz	Cat# sc-8310; RRID:AB_2152867
Rabbit monoclonal anti-phospho-Y705-Stat3	Abcam	Cat# ab76315; RRID:AB_1658549
Rabbit monoclonal IgG	Abcam	Cat# ab172730; RRID:AB_2687931
Rabbit monoclonal anti-SHP2	Cell signaling	Cat# 3752; RRID:AB_2300607
Goat polyclonal anti-MPO	R&D system	Cat# AF3667; RRID:AB_2250866
Rabbit monoclonal anti-cyclinD1	Abcam	Cat# ab134175
Rabbit monoclonal anti-cleaved Caspase-3 (Asp175) (D3E9)	Cell signaling	Cat#9579; RRID:AB_10897512
Rabbit monoclonal anti-Histone H2A.X, phospho (Ser139) (Clone 20E3)	Cell signaling	Cat# 9718; RRID:AB_2118009
Rabbit polyclonal anti-p53 (CM5)	VectorLabs	Cat# VP-P956; RRID:AB_2335917
Mouse monoclonal anti-p53 (DO-1)	Santa Cruz	Cat# sc-126; RRID:AB_628082
Mouse monoclonal anti-p53-HRP (DO-1)	Santa Cruz	Cat# sc-126; RRID:AB_628082
Mouse monoclonal anti-p53 Protein (DO-7)	Dako	Cat# M7001; RRID:AB_2206626
Rabbit polyclonal anti-Stat3 (C-20)	Santa Cruz	Cat# sc-482; RRID:AB_632440
Rabbit monoclonal anti-Stat3 (79D7)	Cell signaling	Cat# 4904; RRID:AB_331269
Rabbit polyclonal anti-HA (Y-11)	Santa Cruz	Cat# sc-805; RRID:AB_631618
Rabbit monoclonal anti-phospho-Jak2 (Y1007+Y1008)	Abcam	Cat# ab32101; RRID:AB_775808
Rabbit monoclonal anti-phospho-Jak2 (Tyr1007/1008) (C80C3)	Cell signaling	Cat# 3776; RRID:AB_2617123
Rabbit monoclonal JAK2 antibody [EPR108(2)]	Abcam	Cat# ab108596; RRID:AB_10865183
Rabbit polyclonal anti-beta-Actin antibody - Loading Control	Abcam	Cat# ab8227; RRID:AB_2305186
Alexa Fluor®488 Goat anti-rabbit IgG (H+L)	ThermoFisher	Cat# A-11034; RRID:AB_2576217
Alexa Fluor®488 Donkey anti-goat IgG (H+L)	ThermoFisher	Cat# A-11055; RRID:AB_142672
Alexa Fluor®647 Donkey anti-rabbit IgG (H+L)	ThermoFisher	Cat# A-31573; RRID:AB_2536183
Peroxidase-AffiniPure F(ab') ₂ Fragment Donkey Anti-Rabbit IgG (H+L)	Jackson ImmunoRes	Cat# 711-036-152; RRID:AB_2340590
Peroxidase-AffiniPure F(ab') ₂ Fragment Donkey Anti-Mouse IgG (H+L)	Jackson ImmunoRes	Cat# 715-036-150; RRID:AB_2340773
ImmPRESS™ Peroxidase polymer reagent	VectorLabs	Cat# MP-7401; RRID:AB_2336529
Bacterial and Virus Strains		
ElectroMAX DH10B cells	Invitrogen/Thermo Fisher Sci.	Cat# 18290-015
Biological Samples		
Patient samples	University Medical Center Göttingen	http://www.chirurgie-goettingen.de/index.php

(Continued on next page)

Continued		
REAGENT or RESOURCE	SOURCE	IDENTIFIER
Chemicals, Peptides, and Recombinant Proteins		
AOM (Azoxy methane)	Sigma	Cat# A5486
DSS (Dextran sodium sulfate)	MP Biomedicals	Cat# 160110
17AAG	provided by NCI	N/A
TAM (Tamoxifen)	Sigma	Cat# T5648
IL-6	ImmunoTools	Cat# 11340064
Napabucasin	Selleckchem	Cat# S7977
Ruxolitinib	Selleckchem	Cat# S1378
Lipofectamine2000	Invitrogen	Cat# 11668-019
Trizol	Invitrogen	Cat# 15596026
Phusion® High-Fidelity DNA Polymerase	Thermo Fisher Sci.	Cat# F530
Critical Commercial Assays		
Proteome Profiler cytokine array	R&D Systems	Cat# ARY028
Invisorb Spin Tissue Mini Kit	Stratec	Cat# 10321003
QuikChange Multi Site-Directed Mutagenesis Kit	Agilent	Cat # 200514
TruSight Tumor 15 Kit (TST15)	illumina	Cat# OP-101-1001
EnVision™ Flex+, Mouse, high pH (Link)	Dako	Cat# K8002
EnVision™ Flex+, Rabbit, high pH (Link)	Dako	Cat# K8009
EnVision™ FLEX Target Retrieval Solution, low pH	Dako	Cat# K800521-2
Cell Culture Inserts, 8.0µm pore size	Falcon	Cat# 353097
Deposited Data		
Raw and analyzed data	This paper	NCBI BioProject ID PRJNA476326
Experimental Models: Cell Lines		
SW1463	ATCC	Cat# CCL-234™
SW48	Kastrinakis et al., 1995	Summerhayes, Boston
SW837	Sigma	Cat# 91031104
HCT116 p53 ^{-/-}	Bunz et al., 1998	B. Vogelstein, Baltimore
H1299	ATCC	Cat# CRL-5803™
HT-29	DSMZ	Cat# ACC 299
LS1034	ATCC	Cat# CRL-2158
Colo-320	Sigma	Cat# 93051113
SW1116	CLS	Cat# 300348
DLD-1	DSMZ	Cat# ACC 278
Experimental Models: Organisms/Strains		
Mouse: Apc1638N	Fodde et al., 1994	N/A
Mouse: p53null (-/-) (B6.129S2-Trp53 ^{<tm1Tyj>/J})	Jacks et al., 1994 or The Jackson Laboratory	Strain# 002101
Mouse: floxR248Q (floxQ)	Alexandrova et al., 2015	N/A
Mouse: Rosa26CreERT2 (B6.129-Gt(ROSA)26Sor ^{tm1(cre/ERT2)Tyj/J})	The Jackson Laboratory	Strain# 008463
Mouse: C57BL/6NCrl	Charles River	Strain# 027
Oligonucleotides		
Primers for QPCR and genotyping, see below	this paper	Table S1
siRNA TP53 Silencer® Select	Ambion	ID: s605
siRNA TP53 Silencer® Select	Ambion	ID: s607
siRNA PTPN11 Silencer® Select	Ambion	ID: s11526
siRNA PTPN11 Silencer® Select	Ambion	ID: s11525
siRNA PTPN11 Silencer® Select	Ambion	ID: s11524
siRNA Negative Control No. 2 (src2) Silencer® Select siRNA	Ambion	Cat# 4390847

(Continued on next page)

Continued

REAGENT or RESOURCE	SOURCE	IDENTIFIER
Recombinant DNA		
pcDNA3	Invitrogen	Replaced by pcDNA3.1 (+/-)
pcDNA3-p53 R280K	Mihara et al., 2003	PMID: 12667443
pcDNA3-p53 R283W	Mihara et al., 2003	PMID: 12667443
pcDNA3-p53 R249S	Mihara et al., 2003	PMID: 12667443
pcDNA3-p53 R175H	Mihara et al., 2003	PMID: 12667443
pCMV-p53 R273H	Gift by Bert Vogelstein	Addgene plasmid # 16439
pCMV-p53 R248W	Gift by Bert Vogelstein	Addgene plasmid # 16437
pCMV-p53 R248Q	This paper	Cloned from pCMV-p53 R248W using a site-directed mutagenesis kit
Software and Algorithms		
ImageJ software	Open source	https://imagej.net/Welcome PMID 22930834
GraphPadPRISM®	Graphpad Software, Inc.	https://www.graphpad.com/
Image Lab™ Software	Biorad	http://www.bio-rad.com/de-de/product/image-lab-software

CONTACT FOR REAGENTS AND RESOURCE SHARING

Requests for further information, resources and reagents should be directed to and will be fulfilled by the Lead Contact, Ute M. Moll (ute.moll@stonybrook.edu).

The following resources are subject to patent applications and may be shared with research organizations for research-only under a material transfer agreement (MTA) in good faith with the recipient, which may restrict the recipient to make any modifications to this material: Constitutive mutant *TP53*^{R248Q} mouse and conditional mutant *TP53*^{R248Q/flox} mouse, *Trp53*^{-/-} mouse and the Hsp90 inhibitor 17AAG.

EXPERIMENTAL MODELS AND SUBJECT DETAILS**Patient Samples**

Clinical samples (tissue resection specimens, n=98) from previously untreated colorectal carcinoma patients undergoing surgery in the department of General, Visceral and Pediatric Surgery of the University Medical Center Göttingen (UMG, Germany) were included in the study. Translational research was approved (approval number 9/8/08) by the UMG Ethics Committee (<http://www.ethikkommission.med.uni-goettingen.de>). Upon informed consent of all participating patients, formalin-fixed paraffin-embedded samples were prospectively collected from Febr 2000 - Sept 2012. Postoperative treatment was administered in accordance with relevant treatment guidelines. Clinical parameters of patients are provided as summary in [Figure S7A](#).

Mouse Experiments and Genotyping

Experiments using animal materials were approved by institutional (Göttingen University Medical Center Ethikkommission) and state (Niedersächsisches Landesamt für Verbraucherschutz und Lebensmittelsicherheit, LAVES, Lower Saxony, Germany) committees, ensuring that all experiments conform with the relevant regulatory standards.

The generation of the humanized constitutive *TP53*^{R248Q} (called p53^Q) and the humanized conditional floxed *TP53*^{R248Q/flox} (called p53^{floxQ}) knock-in alleles has been previously described in detail (Alexandrova et al., 2015; Hanel et al., 2013). Briefly, the human *TP53* sequence containing the R248Q mutation in exon 7 replaces part of the mouse *Trp53* (exons 4-9). In the floxed version, LoxP sites flank this humanized knock-in allele in intron 1 and intron 10. The phenotypes of mice with the p53^Q and p53^{floxQ} alleles are identical (Alexandrova et al., 2015). For [Figures 1, S1, 8, and S8](#), mice with the constitutive p53^Q allele were used. For [Figures 2, S2, 3, S3, 4, and S4](#), mice carrying the p53^{floxQ} allele were used.

To generate heterozygous p53^{floxQ/-} mice and corresponding controls, we crossed mice containing the p53^{floxQ} allele with mice containing the p53-null allele (Jacks et al., 1994). To remove the mutp53 allele with Tamoxifen, we crossed mice containing the p53^{floxQ} allele with *Rosa26CreERT2* ('ERT2') transgenic mice (Ventura et al., 2007).

To genetically induce intestinal tumors, we crossed mice containing the p53^Q allele with *Apc*^{1638N/+} knock-in mice (Fodde et al., 1994) which contain a chain-termination mutation in exon 15 of the murine *Apc*. A p53-null allele was introduced by further crossings with the corresponding mouse strain.

For all genotypings we isolated DNA with Invisorb Spin Tissue Mini Kit (Strattec Molecular). PCR was performed with Phusion® High-Fidelity DNA Polymerase according to the manufacturer's guidelines (ThermoFisher) using the primers specified in [Table S1](#).

All mouse strains were maintained on a C57BL/6 background for at least 6 generations. For experiments, randomly assigned 8 week old males and females weighing at least 20 g were used. Mice were kept under pathogen-free barrier conditions.

Cell Culture and Treatment

Human colorectal cancer cell lines SW48, SW837, SW1463, Colo320, SW480, LS1034, SW1116, DLD-1, HT29 and *TP53*^{-/-} HCT116 were cultured in RPMI 1640 medium. Human lung adenocarcinoma cell line H1299 (*TP53*^{-/-}) were cultured in DMEM. All media were supplemented with glutamine, 10% fetal bovine serum and penicillin/streptomycin. Cell lines were grown in a humidified atmosphere at 37°C with 5% CO₂. HT29 and DLD-1 cells were obtained from the Deutsche Sammlung von Mikroorganismen und Zellkulturen (DSMZ, Braunschweig), SW1463, LS1034 and H1299 from the American Type Culture Collection (ATCC), SW837 and Colo320 from Sigma (Germany), SW48 with *TP53* c.742C>T mutation from Summerhayes Lab in Boston ([Kastrinakis et al., 1995](#)), and *TP53*^{-/-} HCT116 as gift from the Vogelstein Lab (Johns Hopkins University, Baltimore, USA). All cell lines were regularly tested for mycoplasma contamination using the MycoAlert Mycoplasma detection kit (Lonza).

METHOD DETAILS

CRC Induction, Colonoscopy and Treatment

Murine colorectal carcinoma (CRC) was chemically initiated by a single injection of the colon organotropic carcinogen Azoxymethane (AOM), a DNA methylating agent (intraperitoneal AOM, 9.5 mg/kg in 0.9% sodium chloride, Sigma) at the age of 8 weeks. After one week rest, colitis was induced by providing 1.5% (in p53-deficient mice) or 2% (in p53-proficient mice) dextran sodium sulfate (DSS, MP Biomedicals) for 6 days in the drinking water.

While optimizing the AOM/DSS model, we noted a DSS dose-dependent effect in tumor multiplicity depending on whether or not the animals contained at least one WT p53 allele. In p53-proficient heterozygous mice, 'low' DSS concentration (1.5%) generated 6 tumors on average, while 'high' DSS (2%) produced 16 tumors per mouse ([Figure S1D](#)). Thus, for analysis of the more tumor-restrained p53-proficient mice we used 2% DSS in order to achieve a higher tumor burden ([Figures S1E, S1F, and S2A](#)). For the bulk of our studies where we used the more tumor-prone p53-deficient mice which could not tolerate and did not survive 2% DSS, we lowered it to 1.5% DSS (e.g. [Figures 1A–1C, 2, 3, 4, and 8](#)). For analysis of tumor-specific parameters we chose an endpoint study design, terminating at 12 weeks after AOM in mice with the WT p53 allele (e.g. [Figures S1E, S1F, and S2A](#)), and at 10 weeks after AOM in all mice lacking the WT p53 allele (e.g. [Figures 1A–1C](#)). This design also avoided losing mice to extraneous reasons such as intestinal obstruction and anal prolapse in p53-proficient mice, or to lymphoma in p53-deficient mice.

Direct visualization of tumor growth started 5 weeks after AOM induction and was performed by mini endoscopy/colonoscopy (apparatus by Karl Storz GmbH) on anesthetized mice (2% isoflurane inhalation). Tumor sizes were scored according to the Becker & Neurath scoring system ([Becker et al., 2006](#)). Briefly, tumor sizes are determined relative to the width (luminal circumference) of the colon. Individual tumors are scored as sizes 1–5 (S1–S5) with the following specifications: S1 = just detectable, S2 = 1/8 of the lumen, S3 = 1/4 of the lumen, S4 = 1/2 of the lumen and S5 > 1/2 of the lumen.

After visual tumor validation, Tamoxifen (TAM, Sigma) was administered by 7 serial daily intraperitoneal injections (1 mg per injection in an ethanol/oil mixture 1:10) to activate the inducible recombinase (*RosaCreER*^{T2}), causing deletion of the p53^{flloxQ} allele. Tumor growth was monitored by weekly colonoscopy. In some cases tumor biopsies were taken. At endpoints mice were euthanized and the entire colon and rectum were harvested. Colons were longitudinally opened, cleaned and displayed. Tumor numbers were counted and tumor sizes were measured with a caliper. To ensure complete sampling of the organ, each colon/rectum was 'swiss rolled', fixed in 4% paraformaldehyde/PBS and bisected. Both halves were placed face down side-by-side into a single cassette for processing, wax embedding and subsequent tissue analysis.

Pharmacological treatments in [Figures 8 and S8](#) were started at defined scores after tumor visualization by colonoscopy. 17-allyl-17-demethoxygeldanamycin (17AAG) was pre-dissolved in DMSO and further diluted in EPL egg yolk emulsion diluent (10% DMSO/EPL, all provided by the National Cancer Institute). Mice with comparably-sized tumors were treated by intraperitoneal injection with 60 mg/kg of 17AAG or vehicle alone for 5 days per week for 4 weeks. During treatment mice and tumor sizes were monitored by colonoscopy once a week. At endpoint on day 25 mice were prepared as above.

All animal experiments were carried out in full agreement with the guidelines outlined above.

Histological Analysis

Standardized immunohistochemical stainings were performed on murine formalin-fixed paraffin-embedded (FFPE) tissues. The following primary antibodies were used: p53 FL393 (Santa Cruz, sc-6243), Ki67 (Abcam, ab15580), pan-Cytokeratin (Abcam, ab9377), NF-κB p65 (D14E12) (Cell Signaling, #8242), iNOS (NOS2, Santa Cruz, sc-8310), phospho-Y705 Stat3 (Abcam, ab76315), cleaved Caspase 3 (Asp175) (D3E9) (Cell Signaling, #9579) and CyclinD1 (Abcam, ab134175), α-smooth muscle actin/SMA (Abcam, ab21027), Laminin (Abcam, ab11575) and anti-myeloperoxidase/MPO (R&D Systems, AF3667). The ImmPRESS™ (Peroxidase) polymer reagent (Vectorlabs; based on 3, 3'-diaminobenzidine, DAB), or Alexa Fluor®488-coupled and Alexa Fluor®647-coupled secondary antibodies (immunofluorescence) were used as detection systems. Hematoxylin (DAB) or DAPI (immunofluorescence) were used as counterstains. Quantification of positively stained cells was done by counting 3–5 random fields

of 2 sections each per colon at 40x magnification using the CellCounter function of ImageJ software. The percentage of positive malignant epithelial or stromal nuclei relative to the total number of malignant epithelial or stromal nuclei was calculated, and differences between samples were analyzed for statistical significance using Student's *t* test (Excel).

Analogous to the TNM human colorectal cancer staging system, we define mouse CRC tumor stages in this study as follows: T0 = Carcinoma-in-situ, intramucosal only, tumor has not broken through the muscularis mucosae, T1 = cancer has grown through the muscularis mucosae into the submucosa, T2 = cancer has grown through the muscularis mucosae and submucosa into the muscularis propria, T3 = cancer has grown into the outermost layers of the colon or rectum and reached the serosa but has not spread to nearby lymph nodes (N0) or reached nearby organs and has not spread to distant sites (M0).

Intestinal lymphoid aggregates were quantitated under the microscope at 10x magnification by counting the number of aggregates in the intestinal wall on 4 widely separated 4 μ m-thick H&E sections per colon roll. The distance between two subsequent sections was at least the equivalent of one hundred 4 μ m sections to exclude double counting.

Plasmids and Reagents

Plasmids were transfected with Lipofectamine 2000 (Invitrogen). siRNAs to deplete human p53 were purchased from Ambion/Thermo Fisher Scientific (validated Silencer select® siRNAs, ID: s605 and s607 and control scramble2) and transfected with Lipofectamine 2000. IL6 treatment (20 ng/ml, ImmunoTools) was used where indicated. Napabucasin (BBI-608) and Ruxolitinib were purchased from SelleckChem.

Immunoblots, Co-immunoprecipitation (Co-IP), Cytokine Assays

Whole cell lysates were made with RIPA buffer (1% TritonX-100, 1% Desoxycholate, 0.1% SDS, 150 mM NaCl, 10 mM EDTA, 20 mM Tris-HCl pH7.5 and complete protease inhibitor mix, Roche). Tumor tissues were minced and lysed with RIPA buffer followed by sonication. After centrifugation protein concentrations were measured by BCA protein assay (Pierce). For immunoblotting equal amounts of protein lysates were separated by SDS-polyacrylamide gel electrophoresis (PAGE), transferred onto nitrocellulose membranes (Millipore), blocked with 5% milk dissolved from powder and probed with the following antibodies: p53 (CM5, Vector Laboratories) for murine p53, p53 (DO-1, Santa Cruz sc-126) for human p53, Hsc70 (B-6, Santa Cruz sc-7298), phospho-Y705 Stat3 XP (Abcam, ab76315), total Stat3 (Santa Cruz, sc-482) or total Stat3 (79D7) (Cell Signaling, #4904), phospho-Jak2 (Tyr1007/1008) (C80C3) (Cell Signaling #3776), Jak2 (Abcam, ab108596), cyclinD1 (Abcam, ab134175) and Actin (Abcam, ab8227).

For Co-IP cells were lysed in NP40 buffer (50 mM Tris-HCl, pH 7.4, 150 mM NaCl₂, 1% Nonidet P40, 5 mM EDTA, and complete protease inhibitor mix, Roche) followed by sonification. After centrifugation samples were precleared with protein G Sepharose (GE) and equal amounts of total protein were immunoprecipitated with antibodies to phospho-Y705 Stat3 (Abcam, ab76315), total Stat3 (Santa Cruz, sc-482), SHP2 (Cell Signaling #3752) and control IgG antibody (Abcam). For co-IPs, p53 was immunoblotted with an HRP-coupled p53 antibody (Santa Cruz #126). Precipitates were analysed by immunoblotting. An aliquot of each lysate was used as input control.

The Proteome Profiler cytokine array (R&D Systems) was probed with tumor tissue lysates (pooled samples with $n \geq 5$ tumors per group) according to the manufacturer's guidelines.

Quantitative PCR

Total RNA from cells or tumor tissues was isolated using the Trizol reagent (Invitrogen/Thermo Fisher Scientific). Tumor tissues were first homogenized with a handheld homogenizer (T10 basic ULTRA-TURRAX). Equal amounts of RNA were reverse-transcribed (M-MuLV Reverse Transcriptase from NEB), and real-time PCR analysis was performed using a qPCR Master-Mix (75 mM Tris-HCl pH 8.8, 20 mM (NH₄)₂SO₄, 0.01% Tween-20, 3 mM MgCl₂, SYBR Green 1:80,000, 0.2 mM dNTPs, 20 U/ml Taq-polymerase, 0.25% TritonX-100, 300 mM Trehalose). Primers are specified in [Table S1](#).

Scratch Assay

24 hr after transfection with human p53 R248Q expression plasmid or empty control vector cells were continuously treated with IL6 (20 ng/ml) or left untreated in serum-reduced media (1% FCS). 48 hr post transfection, three scratches per well were made using a 1 ml pipette tip for H1299 cells and a 200 μ l pipette tip for *TP53*^{-/-} HCT116 cells. Cells were treated or not treated with Stat3 inhibitor BBI-608 (500 nM). 24 hr after scratching, at least 5 images per scratch were taken and the wound healing area was measured with ImageJ software.

Transwell Migration Assay

Cells were transfected with human p53 R248Q plasmid or empty control vector and continuously treated with IL6 (20 ng/ml) or left untreated. 48 hr after transfection cells were trypsinated and 50,000 cells were loaded per transwell insert (8.0 μ m pore size, Falcon) in serum-reduced media. Wells were filled with complete medium +/- IL6. 24 hr after loading, the cells that had migrated to the underside of the membrane were fixed in methanol for 10 min and stained with crystal violet (0.1% in 20% EtOH for 20 min). After washing, remaining cells in the insert were removed. Migrated cells were visualized by light microscopy and counted with Image J. Migration rates were calculated relative to vector-only transfected cells.

Fluorescent In Situ Hybridization (FISH)

Paraffin-embedded colons were sectioned with 5 μm thickness, de-waxed and hydrated following standard procedures. Sections were incubated with pan-bacterial Cy5-conjugated EUB338 probe (5'-GCTGCCTCCCGTAGGAGT-3') for the detection of all bacteria. A non-sense probe (5'-CGACGGAGGGCATCCTCA-3') conjugated to Cy3 (NON338) was used as negative control. Both probes (Eurofins Genomics) were applied to slides at a concentration of 0.5 μg in prewarmed hybridization buffer (900 mM NaCl, 20 mM Tris pH 7.5, 0.01% SDS, 20% formamide). Slides were incubated at 46°C in a humid chamber for 2 hr and washed at 48°C for 2 x 15 minutes in wash buffer (215 mM NaCl, 20 mM Tris pH 7.5, 5 mM EDTA). Slides were rinsed in distilled water and coverslips were mounted using ProLong Gold antifade reagent with DAPI (Thermo Fisher Scientific). For each colon, the average number of intratumoral bacteria was determined by scoring the number of bacteria from at least 10 different regions of a random section. Slides were imaged using a Zeiss Axio Imager with AxioVision software.

Quantitative Immunohistochemistry on Patient Samples

Freshly resected tumor samples from patients were immediately fixed in 4% buffered formalin, subjected to a standard ethanol dehydration series, and embedded in paraffin. Immunohistochemistry was performed on 2 μm tissue sections on a Dako Autostainer Link 48 with standardized settings. Sections were incubated in EnVision Flex Target Retrieval Solution (Dako, Hamburg, Germany) and then stained with primary antibodies against phospho-Y1007/1008-Jak2 (Abcam, ab32101), phospho-Y705-Stat3 (Abcam, ab76315) and p53 (clone DO-7) (Dako, IR61661-2) at standardized concentrations for 30 minutes at room temperature. Subsequently sections were incubated with polymeric secondary antibodies coupled to horseradish peroxidase (EnVision Flex+, Dako). Sections were developed with 3,3'-diaminobenzidine (DAB, Dako), and counterstained with Meyer's hematoxylin. Sections were analyzed by light microscopy (AxioScope, Zeiss) with ZENblue software (Zeiss). Two investigators independently scored all tumor sections for nuclear phospho-Y1007/1008-Jak2, phospho-Y705-Stat3 and p53 staining using a four-stage scoring system based on the number and intensity of stained tumor nuclei (0 = negative; 1 = weakly positive; 2 = median positive; 3 = highly positive).

Specifically, grading for phospho-Y1007/1008 Jak2 and phospho-Y705-Stat3: 0 = <5% of tumor nuclei with low intensity; 1 = 5%-50% with low intensity or 5%-20% with high intensity; 2 = 20%-50% with high intensity and 3 = >50% with high intensity. Groups 0 and 1 were combined to form 'pJak2^{low}', and groups 2 and 3 were combined to form 'pJak2^{high}', respectively. Grading for p53: 0 = negative throughout; 1 = 1%-50% with low intensity or 1%-10% with high intensity; 2 = 10%-50% with high intensity and 3 = >50% with high intensity. Groups 0 and 1 were combined to form 'p53^{low}', and groups 2 and 3 were combined to form 'p53^{high}'. Missense mutant p53 often accumulates in tumor cells due to pronounced stabilization (Yue et al., 2017). Thus, strong p53 accumulation is considered a surrogate marker for the presence of a p53 missense mutation.

RPPA Analysis

We used all publicly available tumor Reverse Phase Protein Array (RPPA) datasets from an unrelated human CRC cohort in The Cancer Genome Atlas (TCGA) to determine whether proteins were differentially expressed in CRC tumors between codon-specific *TP53*^{R248} mutants versus other mutational *TP53* categories (nonsense, all other missense mutations and WT). Protein data were downloaded from the GDAC site (<https://gdac.broadinstitute.org>) of the most recent 2016-01-28 version. Tumor samples with *TP53* mutational information were downloaded from cBioportal. Only overlapping sample IDs that existed in both ICGC and TCGA databases were included in the analysis. We did comparisons for expression levels of pTyr705-Stat3 in CRC tumors with *TP53*^{R248} missense mutations (R248) vs p53 truncations or deletions (nons) vs all non-R248 missense mutations (mis) vs *TP53* WT (wt). Each comparison was done independently by one-tailed Student's t-test. The *TP53*^{R248} mutant tumors uniquely expressed higher levels of pStat3 (Figure 7H).

Survival Analysis of Patient ICGC Data

For survival analysis we downloaded data from the International Cancer Genome Consortium (ICGC) (release # 25, June 2017 DCC.ICGC.ORG). We used advanced search criteria for donors with vital status (deceased or alive), available data type (SSM, simple somatic mutation) and the *TP53* gene. Among 3,418 patients identified, 2,194 patients exhibited *TP53* simple somatic mutations of which 191 patients carried R248 missense mutations and 2,003 patients carried non-R248 missense mutations. Among the 191 R248 patients, 103 patients carried R248Q; 78 patients carried R248W; 5 patients carried R248L; 2 patients carried R248P; 2 patients carried R248G, and 1 patient had an unknown R248 mutation. Kaplan-Meier analysis was performed.

QUANTIFICATION AND STATISTICAL ANALYSIS

Statistical specifications of each experiment such as number of animals, number of tumors, biological replicates, technical replicates, precision measures (mean and \pm SEM) and the statistical tests used are provided in the figures and figure legends.

Unpaired Student's t test was used to calculate the p values for comparisons of tumor numbers, relative mRNA expression levels or quantitative evaluation of immunohistochemical stainings.

Correlation studies of immunohistochemically stained CRC tissue samples were analyzed using the Pearson correlation factor R.

Kaplan-Meier survival analysis was performed using the software GraphPadPRISM® with the Log-rank (Mantel-Cox) test.

Graded and grouped patient samples stained for phospho-Tyr705-Stat3, phospho-Y1007/1008-Jak2 and p53 were sorted and statistically analyzed for correlations with clinical and pathological parameters using the software GraphPadPRISM and Fisher's exact test.

Densitometric measurements for quantification of immunoblot bands were done with the gel analysis software Image Lab™ (Bio-rad) and normalized to loading controls.

The following designations for levels of significance were used within this manuscript: $p^* = 0.05$; $p^{**} = 0.01$; $p^{***} = 0.001$; ns, not significant.

DATA AND SOFTWARE AVAILABILITY

TP53 sequencing of human CRC tumor samples was done with the TruSight Tumor 15 Kit (TST15, Illumina) (Molecular Pathology and Research, UMG Göttingen). Tumor areas on histological sections were diagnosed by a pathologist and macrodissected. FFPE-derived DNA was isolated by Proteinase K treatment and automated extraction using the InnuPureC16 System (Analytikjena, Jena, Germany) following the manufacturer's guidelines was done. For analysis of the next generation sequencing (NGS) data with the program CLC Biomedical Workbench (Quiagen), the *TP53* transcript TP53-201 ENST00000269305 was used as reference. Sequencing data for all 29 cases of human CRC tumors that we analyzed were uploaded to the NCBI BioProject database (BioProject ID: PRJNA476326, SRA ID: SRP150627, URL: <http://www.ncbi.nlm.nih.gov/bioproject/476326>).

Cancer Cell, Volume 34

Supplemental Information

Therapeutic Ablation of Gain-of-Function

Mutant p53 in Colorectal Cancer Inhibits

Stat3-Mediated Tumor Growth and Invasion

Ramona Schulz-Heddergott, Nadine Stark, Shelley J. Edmunds, Jinyu Li, Lena-Christin Conradi, Hanibal Bohnenberger, Fatih Ceteci, Florian R. Greten, Matthias Dobbstein, and Ute M. Moll

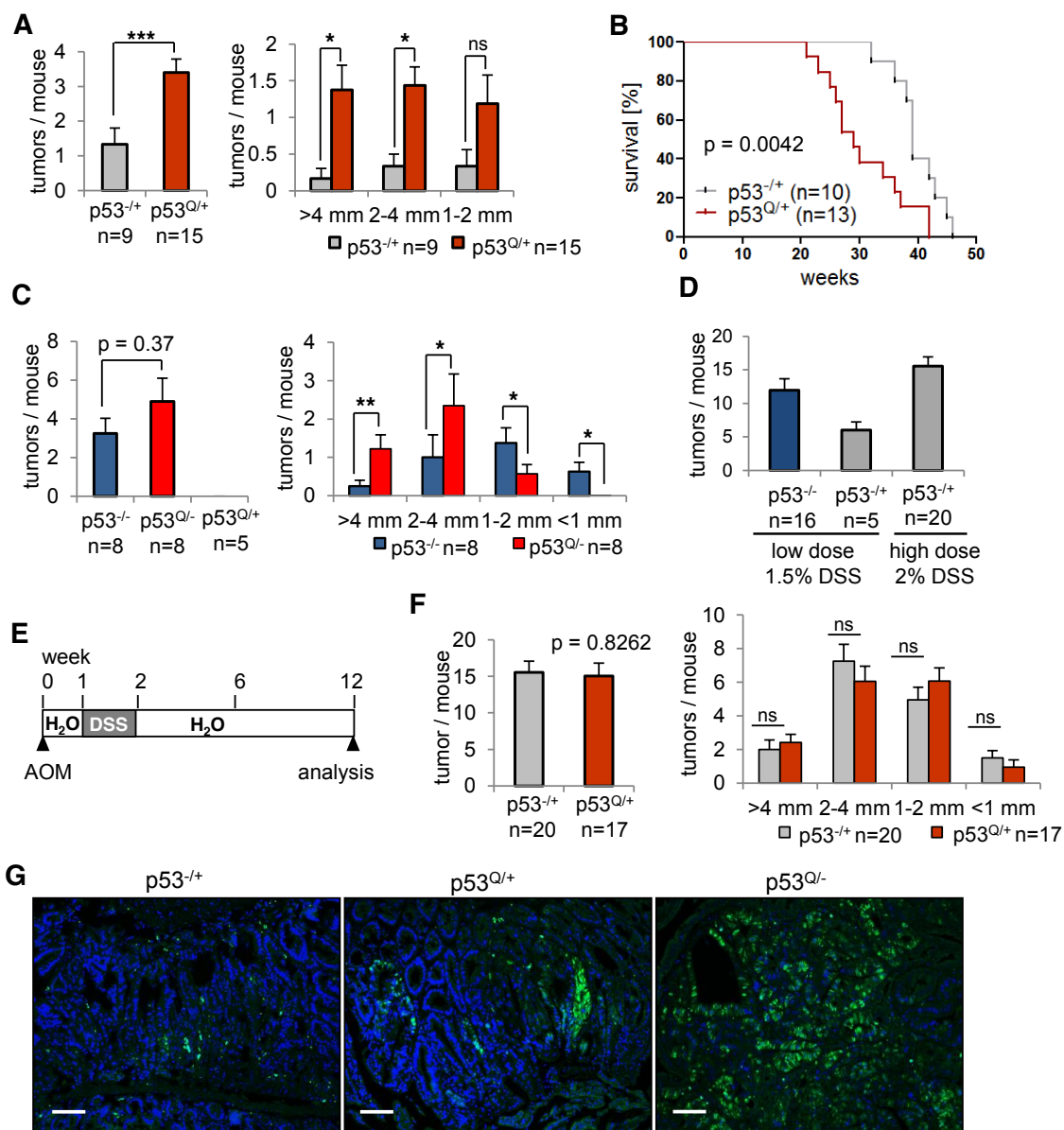


Figure S1. Related to Figure 1. *mutp53* exerts GOF activity in a genetic mouse model of intestinal cancer.

(A) Overall (left) and size dependent (right) tumor frequency in p53^{-/+};Apc^{1638N/+} and p53^{Q/+};Apc^{1638N/+} mice at endpoint 25 weeks of age. This endpoint was chosen because the p53^{Q/+};Apc^{1638N/+} mice start to die at that time point (see survival curve in B).

(B) Kaplan-Meier survival curves of p53^{-/+};Apc^{1638N/+} and p53^{Q/+};Apc^{1638N/+} mice. p53^{Q/+};Apc^{1638N/+} mice died 10 weeks earlier (median survival 29 weeks vs 39 weeks for p53^{-/+};Apc^{1638N/+} controls). Log-rank test, animal numbers are indicated, p = 0.0042.

(C) Tumor frequency as in A, but in the absence of a WT p53 allele. p53^{-/-};Apc^{1638N/+} and p53^{Q/-};Apc^{1638N/+} mice were assessed at 16 weeks of age. The earlier time point was chosen to avoid losing mice to subsequent lymphoma development. For comparison, at 16 weeks of age, p53^{Q/+};Apc^{1638N/+} mice had not yet developed intestinal tumors.

(D) Dose finding of DSS. Treatment with low dose (1.5%) or high dose (2%) of DSS in the drinking water after a single bolus of AOM administration. Tumor numbers per mouse in p53^{-/-} and p53^{+/-} mice at endpoint 10 weeks after AOM/DSS treatment. Since p53^{-/-} mice did not survive a high dose of 2% DSS (data not shown), we used 1.5% DSS for p53-deficient (p53^{Q/-} and p53^{-/-}) mice throughout this study.

(E) Time line of the AOM/DSS (2%) colorectal cancer model in p53-proficient mice (containing one WTp53 allele) used in this study. Endpoint at 12 weeks.

(F) Tumor frequency in p53^{+/-} and p53^{Q/+} mice at 12 weeks after AOM/DSS treatment (scheme in E). An endpoint of 12 weeks was a compromise that ensured large tumor size, yet curtailed the risk of subsequent intestinal obstruction that both genotypes became prone to beyond 12 weeks.

(A, C, D, F) n = number of mice. Mean ± SEM, Student's t-test. p* = 0.05; p** = 0.01; p*** = 0.001; ns, not significant.

(G) Representative p53 immunofluorescence staining (green) of intestinal tumor sections from *Apc*^{1638N/+} mice of the indicated p53 genotypes at endpoints 16 weeks (p53^{Q/-}) and 25 weeks (p53^{+/-} and p53^{Q/+}), respectively. DAPI counterstain (blue). Scale bars 100 μm.

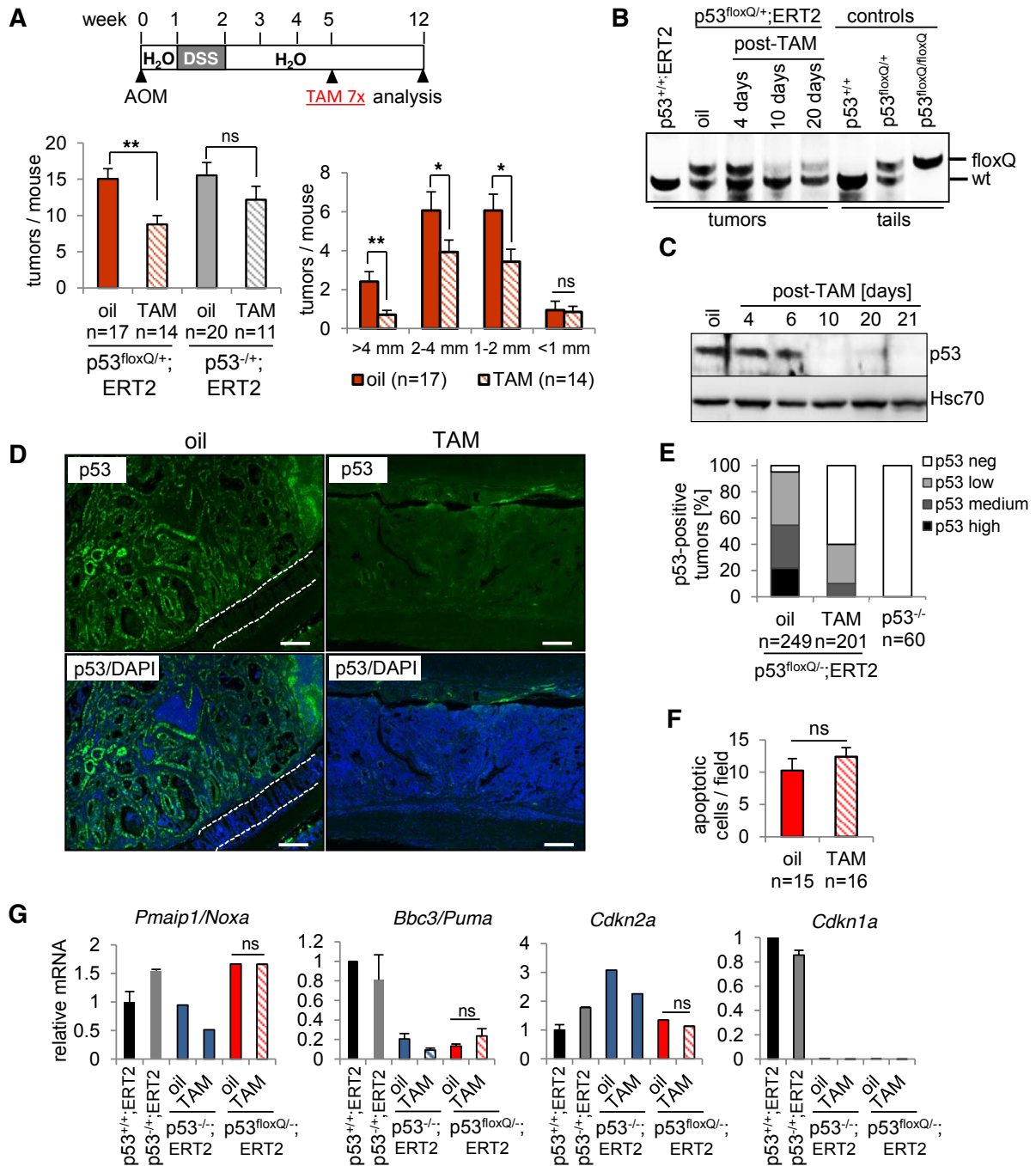


Figure S2. Related to Figure 2. **Genetic ablation of the inactivatable hotspot mutp53 allele $p53^{floxQ}$ inhibits tumor growth.**

(A) The AOM/DSS (2%) treatment scheme used for p53 heterozygous mice. Tamoxifen (TAM) or oil treatment was administered by 7 serial daily intraperitoneal injections at 5 weeks post AOM when each mouse had at least 2-3 S1 tumors and one S2 or larger tumor confirmed by colonoscopy and scored according to Becker & Neurath (Becker et al., 2006). Total (left) and size-dependent (right) tumor numbers per mouse in $p53^{floxQ/+};ERT2$ and $p53^{-/-};ERT2$ mice are plotted. n = number of mice. Mean \pm SEM, Student's t-test. $p^{**} < 0.01$, $p^* < 0.05$.

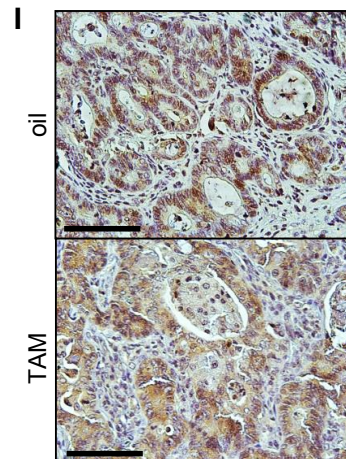
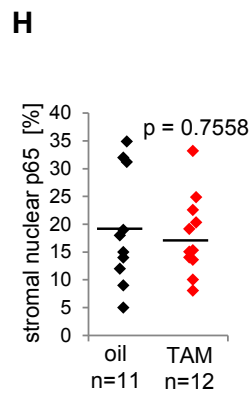
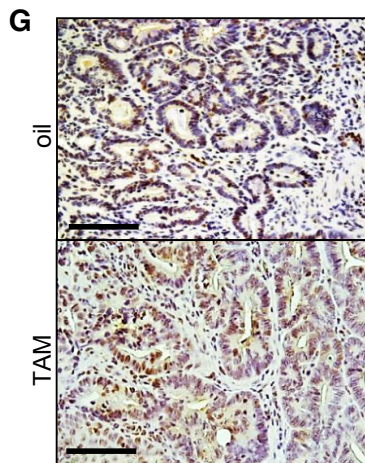
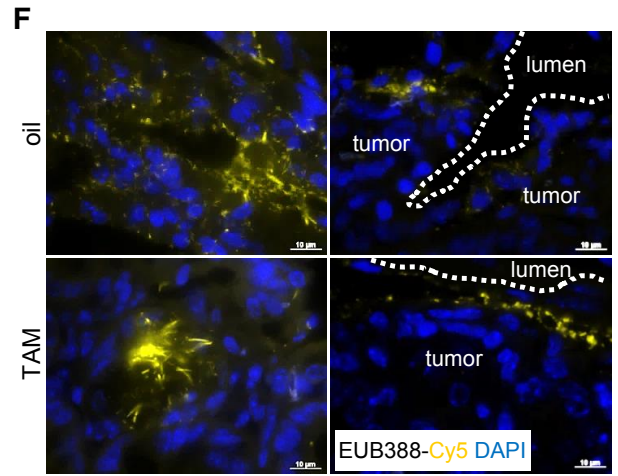
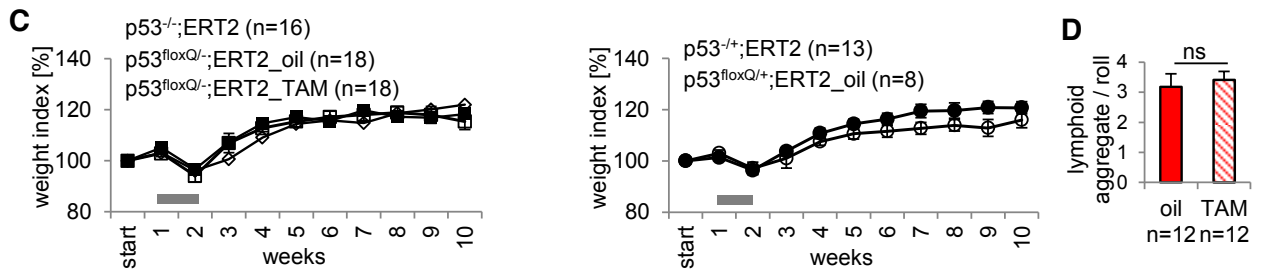
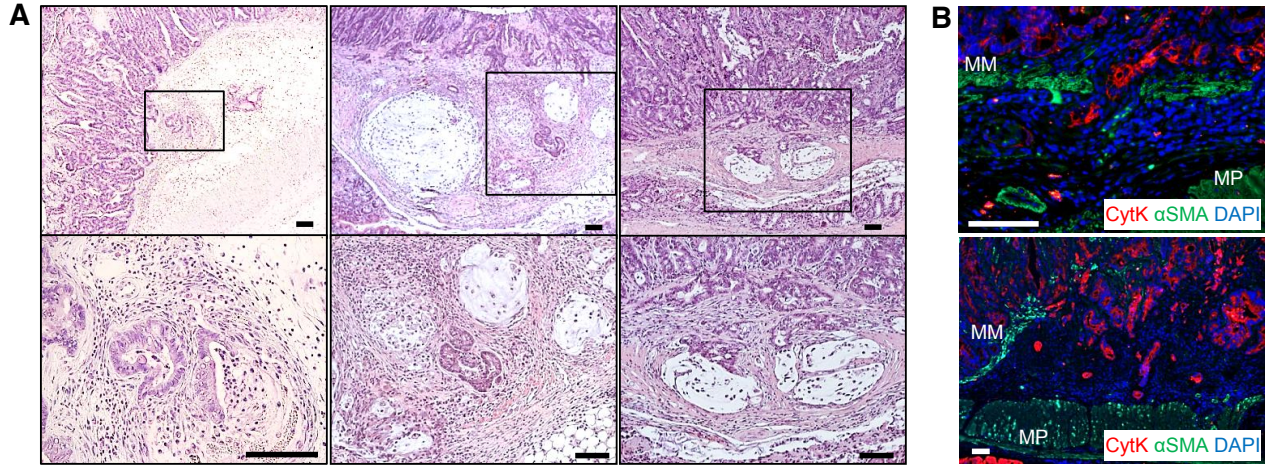
(B) Validation of TAM-induced removal of the p53^{flloxQ} allele. Genotyping PCR of tumors from p53^{flloxQ/+};ERT2 mice treated with oil or TAM. Tumor DNA was isolated at the indicated time points after the first day of TAM administration (post-TAM). Tail biopsies of the indicated genotypes served as allele controls.

(C) Loss of detectable mutp53 protein upon removal of the p53^{flloxQ} allele by TAM treatment. Immunoblot analysis of colonic tumors. Protein was isolated from tumors at the indicated time points post-TAM as in (B). Hsc70, loading control.

(D, E) Efficiency of mutp53 protein removal by TAM treatment. Representative p53 immunofluorescence images (green) of tumor sections from oil- and TAM-treated p53^{flloxQ/-};ERT2 mice at 10 weeks after AOM/DSS (D). Cell nuclei were counterstained by DAPI (blue). Dashed lines delineate a stretch of normal colon present in the same cross-section of the Swiss role, indicating a lack of mutp53 stabilization in normal epithelium of these knock-in mice. Scale bars 100 μ m. n = number of mice. Quantitation of p53-stained tumors (E) was performed in all tumors of the indicated groups at 20x magnification. 'p53 high' indicates that more than 60% of the tumor cells were p53-positive, 'p53 medium' corresponds to 30-60%, 'p53 low' to 5-30% and 'p53 neg' to less than 5%. Percentage of staining was averaged from all tumors for each subgroup. n = number of mice. For the oil group 249 tumors from 17 mice were scored; for the TAM group 201 tumors from 16 mice were scored and for the p53^{-/-} group 60 tumors from 10 mice were scored.

(F) Analysis of apoptosis upon mutp53 ablation. Cleaved caspase 3 was detected by immunostaining of tumor sections from oil- and TAM-treated p53^{flloxQ/-};ERT2 mice at 10 weeks after AOM. At 40x magnification, apoptotic cells were quantified for 5 random fields each. Fifteen tumors from 5 oil-treated mice and 16 tumors from 5 TAM-treated mice were counted. Mean \pm SEM. Student's t-test.

(G) Analysis of gene expression changes upon mutp53 ablation. Relative levels of the indicated mRNAs, isolated from tumors of the indicated groups at 10 weeks (for WTp53-deficient) or 12 weeks (for WT p53-proficient) mice after AOM/DSS treatment. n \geq 5 tumors per group, qRT-PCR normalized to 36B4 mRNA. Relative expression levels are provided as [ratio ($2^{-\Delta\Delta CT}$)]. Mean \pm SEM. Student's t-test. ns, not significant. Note that *Cdkn1a/p21* mRNA levels were essentially zero and do not show on the plot.



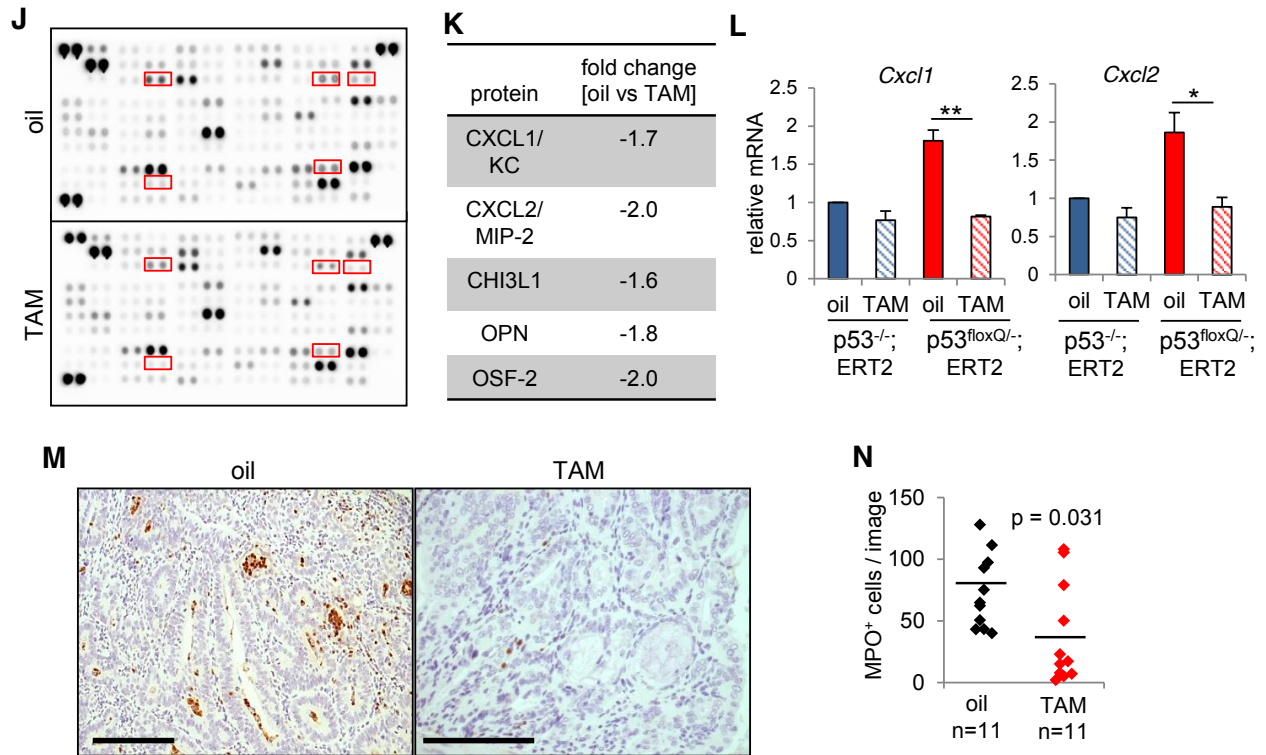


Figure S3. Related to Figure 3. Invasion in colorectal cancer strongly depends on stabilized mutp53.

(A) Invasion of tumors expressing mutp53. Representative histologic sections of oil-treated $p53^{flloxQ/-};ERT2$ colons at 10 weeks after AOM/DSS. Rectangles indicate the enlarged areas shown in the bottom row. Scale bars 100 μ m. H&E staining.

(B) Representative immunofluorescence staining for alpha-Smooth Muscle Actin (α -SMA, smooth muscle marker, green), pan-cytokeratin (CytK, epithelial marker, red) and DAPI (blue) of invasive tumors from oil-treated $p53^{flloxQ/-};ERT2$ mice at endpoint 10 weeks after AOM/DSS. Scale bars 100 μ m. MM, muscularis mucosae. MP; muscularis propria.

(C) Transient weight loss upon AOM/DSS treatment. Mice of the indicated genotypes were treated (grey bars indicate the week of DSS) and body weight was measured weekly until endpoint at 10 weeks. Values were normalized to starting weight set at 100% and shown as mean \pm SEM.

(D) Lymphoid aggregates per colon from oil- and TAM-treated $p53^{flloxQ/-};ERT2$ mice at 10 weeks after AOM/DSS. The number of intestinal lymphoid aggregates on 4 widely separated 4 μ m thick H&E sections per colon Swiss roll tissue block were counted using 10x magnification. The distance between two subsequent sections was at least the equivalent of one hundred serial sections to exclude double counting. Mean \pm SEM, Student's t-test.

(E) Representative invasive fronts of oil- and TAM-treated $p53^{flloxQ/-};ERT2$ tumors at 10 weeks after AOM/DSS. Immunostaining for pan-cytokeratin (panCytK) highlights the invading glands (black arrowheads). Dashed lines and stars indicate muscularis mucosae. The same degree of inflammatory infiltrate exists in both groups. Scale bars 100 μ m.

(F) Bacterial infiltrates in tumor tissues. Fluorescence in-situ hybridization analysis of oil- and TAM-treated $p53^{flloxQ/-};ERT2$ tumors at 10 weeks after AOM/DSS using a Cy5-labeled universal eubacterial probe (EUB 338). See Figure 3L for quantitation. Scale bars 10 μ m.

(G, H) Representative nuclear NF- κ B p65 immunostaining of oil- and TAM-treated p53^{flloxQ/-};ERT2 tumors at 10 weeks after AOM/DSS (G). Scale bars 100 μ m. See Figure 3M for quantitation of tumor epithelial cells with NF- κ B p65-positive nuclei. Quantitation of stromal cells with NF- κ B p65-positive nuclei as percentage of total stromal nuclei (H). Four random fields (at 40x magnification) of 2 standardized IHC tumor sections each were counted per colon. Number of NF- κ B p65-positive nuclei as percentage of total nuclei. For oil (black) 11 tumors from 4 mice and for TAM (red) 12 tumors from 5 mice were counted. Black lines, mean. Student's t-test.

(I) Immunohistochemical staining for iNOS in CRC tumors from oil-treated and TAM- treated p53^{flloxQ/-};ERT2 mice at 10 weeks after AOM/DSS induction. Scale bars 100 μ m.

(J, K) Proteome cytokine array of 111 inflammatory regulators (dot blot replica, each in duplicate) from tumor lysates of oil-treated or TAM-treated p53^{flloxQ/-};ERT2 mice at 10 weeks after AOM/DSS (J). Pooled samples from $n \geq 5$ mice per group. Red rectangles indicate the 5 inflammatory regulators undergoing changes in spot pixel density between treatment groups. Expression profiles of mean spot pixel densities were created by image analysis software and calculated as relative fold changes (K).

(L) Relative expression levels of the indicated mRNAs isolated from tumors of the indicated groups ($n \geq 5$ tumors per groups) at 10 weeks after AOM/DSS. qRT-PCRs were normalized to 36B4 mRNA. Relative values are provided as [ratio ($2^{-\text{ddCT}}$)]. Mean \pm SEM. Student's t-test, $p^{**} < 0.01$, $p^* < 0.05$.

(M, N) Representative immunostaining for neutrophil marker myeloperoxidase (MPO) of oil- and TAM-treated p53^{flloxQ/-};ERT2 tumors at 10 weeks after AOM/DSS (M). Scale bars 100 μ m. Quantitation of MPO positive cells per image (40x magnification) (N). Four random fields of 2 standardized IHC tumor sections per colon were counted. For oil (black) 11 tumors from 5 mice and for TAM (red) 11 tumors from 5 mice were counted. Black lines, mean. Student's t-test.

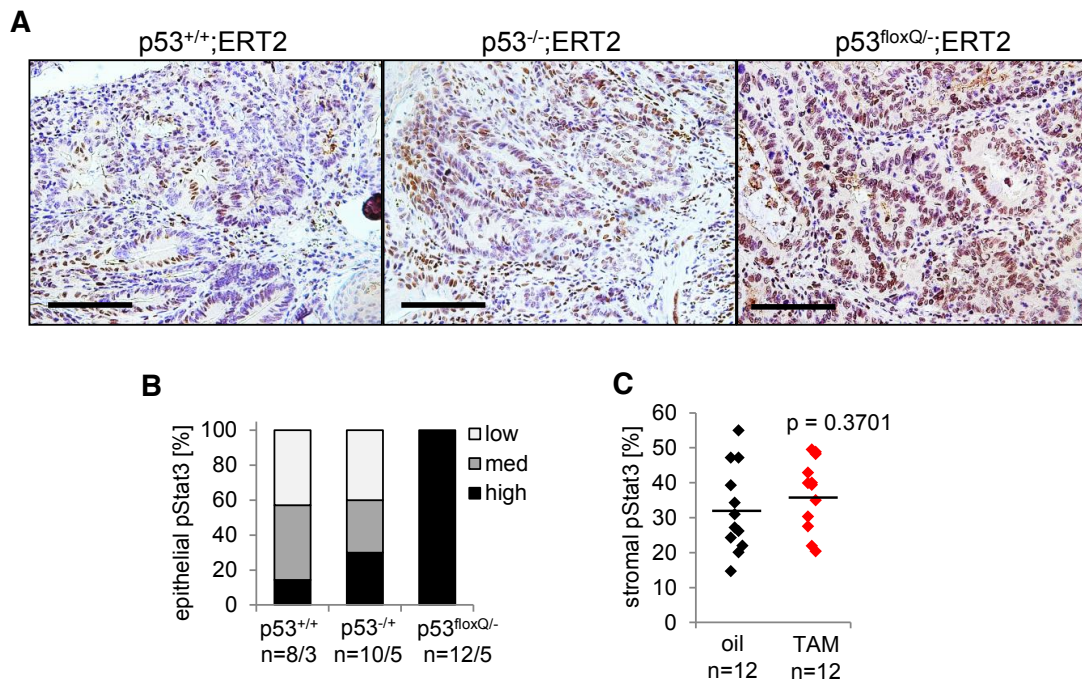


Figure S4. Related to Figure 4. **GOF mutp53 strongly enhances epithelial Stat3 activity far beyond that of WT p53-deficient colorectal cancer cells.**

(A, B) Representative images of standardized immunostaining for pTyr705-Stat3 (pStat3) in CRCs of the indicated genotypes at 10 weeks after AOM/DSS (A). Scale bars 100 μ m. Quantitation of tumor cell nuclei staining positive for pStat3 (B). Analysis of 4 random fields at 40x magnification from 2 tumor sections per colon. 'pStat3 high' indicates that more than 50% of the tumor epithelial nuclei stain strongly positive, 'pStat3 med' (medium) refers to 20-50% and 'pStat3 low' to 5-20%. The percentage of pStat3 staining was averaged from all tumors for each group. n = x tumors out of y mice.

(C) Quantitation of stromal cells with pStat3-positive nuclei of the immunostainings performed in (A). Four random fields at 40x magnification from 2 tumor sections per colon were counted. Positive stromal nuclei as percentage of total stromal nuclei are indicated. For oil (black) 12 tumors from 6 mice and for TAM (red) 12 tumors from 6 mice were counted. Black lines indicate the mean. Student's t-test.

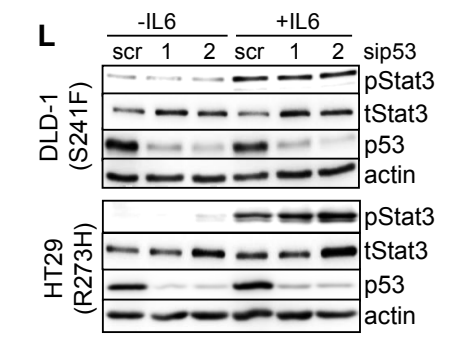
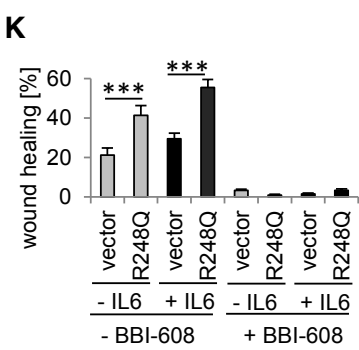
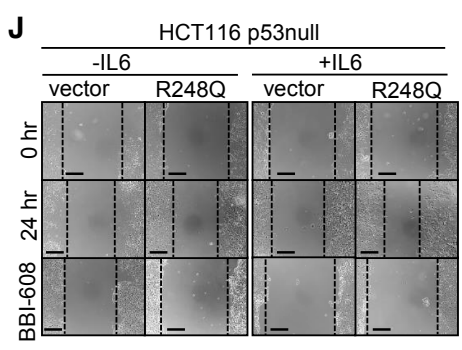
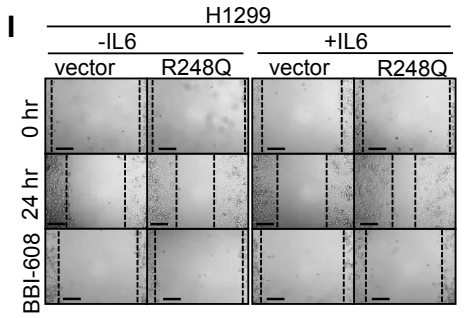
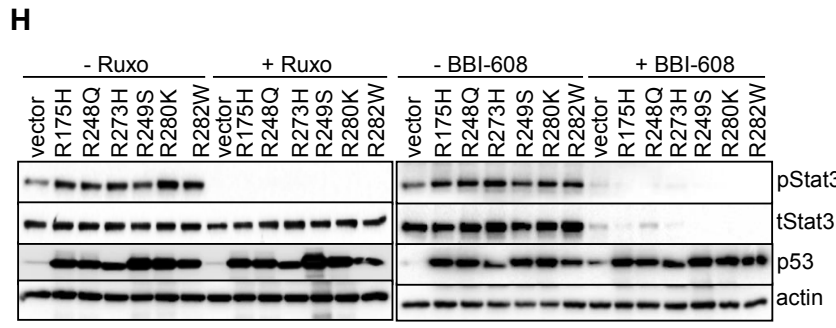
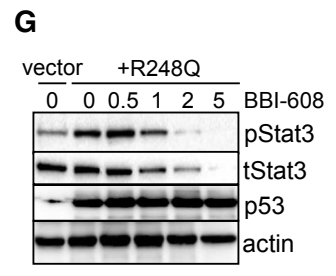
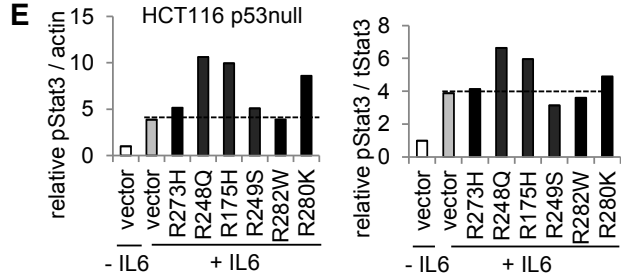
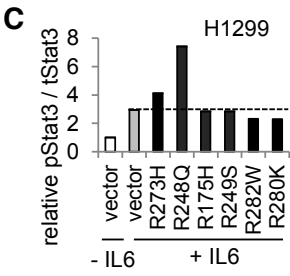
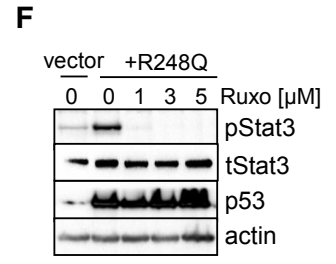
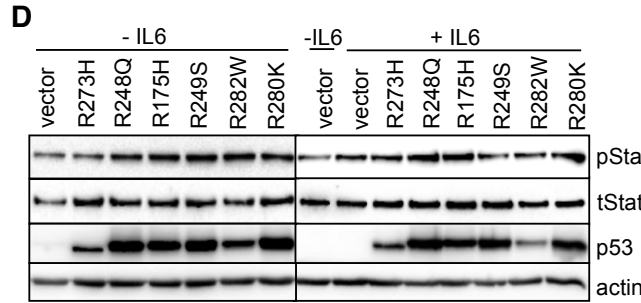
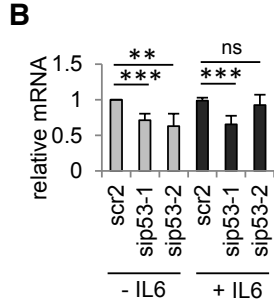
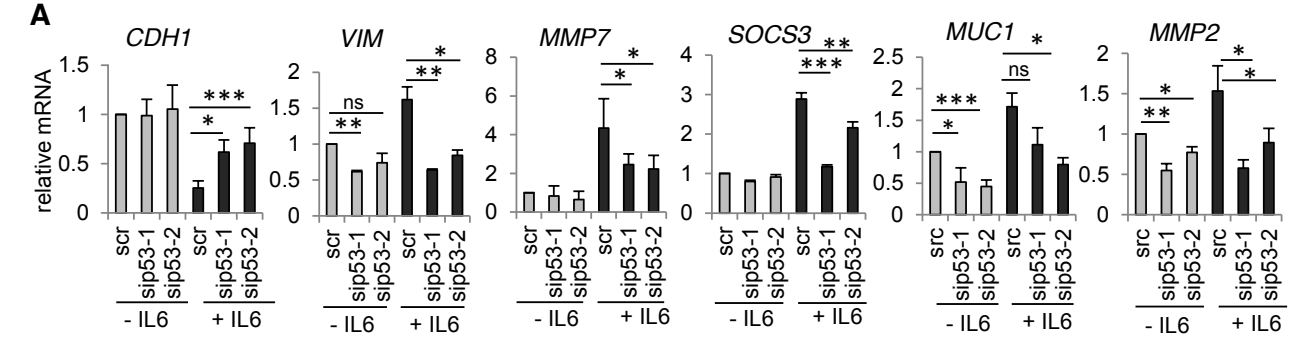


Figure S5. Related to Figure 5. mutp53 activates Stat3 phosphorylation in human CRC cells, resulting in EMT and cell migration.

(A) Relative levels of the indicated mRNAs. Knockdown of endogenous mutp53 by two different siRNAs in human CRC SW48 cells (harboring *TP53^{R248W}*). 24 hr after transfection with two different p53 siRNAs or scrambled (scr) control, cells were IL6-treated for 72 hr or left untreated.

(B) Relative levels of *CCNB1* mRNA. Knockdown of endogenous mutp53 by two different siRNAs in human CRC SW48 cells as in (A).

(A, B) qRT-PCR results were normalized to 36B4 mRNA. Error bars indicate the mean \pm SEM of two independent experiments, each performed in parallel triplicates. Student's t-test, $p^* = 0.05$; $p^{**} = 0.01$; $p^{***} = 0.001$.

(C) Densitometric measurements of the immunoblot in Figure 5C, right panel. The dashed line indicates the level of IL6-only activated pStat3 as reference.

(D) Expression of p53 hotspot mutants in *TP53^{-/-}* HCT116 cells, a human CRC cell line. 48 hr after transfection with expression plasmids, cells were IL6-treated for 24 hr or left untreated. Immunoblot analysis. Vector, empty backbone plasmid. Actin, loading control.

(E) Densitometric measurements of the immunoblot in (D), right panel. The dashed line indicates the level of IL6-only activated pStat3 as reference.

(F, G) Expression of the hotspot mutant p53 R248Q in *TP53^{-/-}* HCT116 cells. 48 hr after transfection with expression plasmids or empty vector, cells were treated with the Jak2 inhibitor Ruxolitinib (Ruxo) (F) or the Stat3 inhibitor BBI-608 (G) at the indicated concentrations in μ M for 24 hr. Immunoblot analysis. Actin, loading control.

(H) Expression of p53 mutants in *TP53^{-/-}* HCT116 cells as in (D), but treated with 1 μ M Ruxolitinib (Ruxo) or 2 μ M BBI-608 for 24 hr. Immunoblot analysis. Actin, loading control.

(I) Representative images of the scratch assay from Figure 5E with *TP53^{-/-}* H1299 cells expressing the p53 R248Q mutant. 24 hr after transfection with p53 R248Q plasmid or control vector, cells were continuously treated with IL6 or left untreated in serum-reduced media (1% FCS). 48 hr after transfection, three scratches per well were made in duplicates with a 1 ml pipette tip. Simultaneously, cells were treated or not treated with Stat3 inhibitor BBI-608 (500 nM). Wound healing images were taken 24 hr after scratching. For Figure 5E, at least 5 images per scratch were taken, the area was measured with Image J and migration rate was calculated. Scale bars, 200 μ m.

(J, K) Representative images of scratch assays with *TP53^{-/-}* HCT116 cells expressing the R248Q mutant (J). Assay was performed as described in (I). Wound healing after 24 hr. Scale bars, 200 μ m. At least 5 images per scratch were taken, the area was measured with Image J and migration rate was calculated (K). Error bars indicate \pm SEM of 2 independent experiments in duplicates. Student's t-test, $p^{***} = 0.001$.

(L) Stat3 signaling upon knockdown of endogenous mutp53 by two different p53 siRNAs or scrambled (scr) control sequences in the indicated human colorectal cancer cell lines as in Figure 5A. In contrast to CRC cell lines with highly expressed mutp53 R248 proteins, CRC cells with low levels of mutp53 (see Figure 5G) do not show a dependency of pStat3 levels on mutp53. 48 hr after transfection cells were treated with IL6 or left untreated for 24 hr. Immunoblot analysis. Actin, loading control.

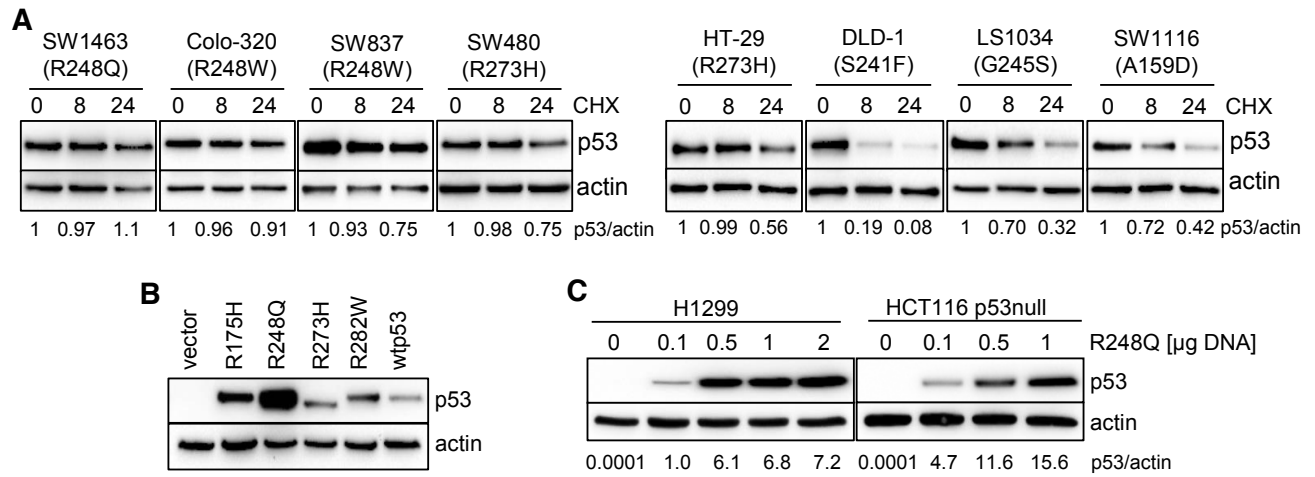


Figure S6. Related to Figure 6. **Highly stabilized mutp53 constitutively activates Stat3 phosphorylation by physical interaction with pStat3, displacing the SHP2 phosphatase.**

(A) Cycloheximide (CHX, 40 μ g/ml) chases of the indicated CRC cell lines immunoblotted for p53. Actin, loading control. Densitometric measurements are shown below.

(B) Comparative ectopic expression of p53 hotspot mutants in *TP53*^{-/-} HCT116 cells. 48 hr after transfection with 200 ng expression plasmid per mutant, cells were analyzed by immunoblot. Vector, empty backbone plasmid. Actin, loading control.

(C) Comparative expression of p53 R248Q plasmid in *TP53*^{-/-} H1299 and *pTP53*^{-/-} HCT116 cells. 48 hr after transfection with the indicated amounts of expression plasmid or empty backbone vector, cells were analyzed by immunoblot. Actin, loading control. Densitometric measurements of immunoblots are shown below.

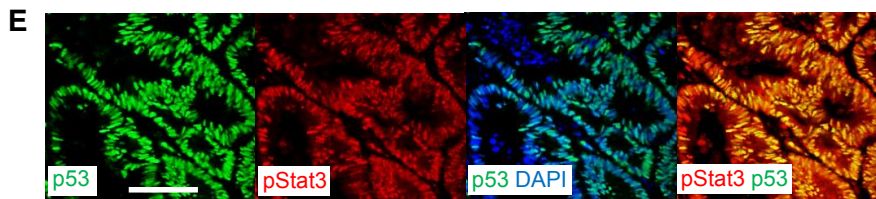
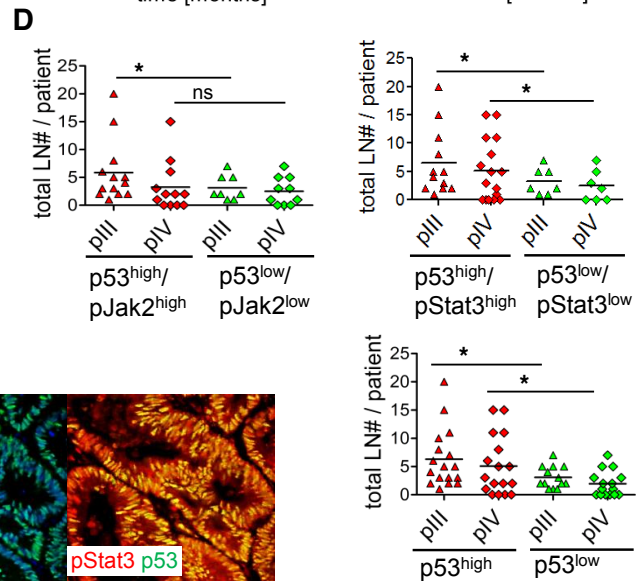
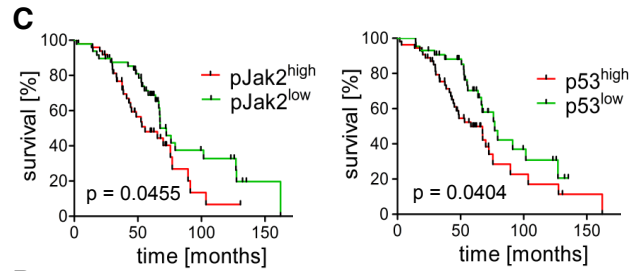
A Characteristics of patients

Characteristic	Value (n=98)	%
Male/Female ratio	65:33=1.96	n.a.
Median/range age	64(45-87)	n.a.
pJak2, pStat3 and p53 level		
pJak2 ^{high}	54	55.1
pJak2 ^{low}	44	44.9
pStat3 ^{high}	62	63.2
pStat3 ^{low}	36	36.7
p53 ^{high}	55	56.1
p53 ^{low}	43	43.9
Tumor site		
Colon/Sigma	32	31.9
Rektum	66	68.1
Pathological T-stage		
I	11	11.3
II	24	24.7
III	30	30.9
IV	32	32.9
Pathological N-category		
pN0	45	46.4
pN1/2	53	53.6
Distant Metastases		
M0	66	67.0
M1	32	33.0
Histopathological grading		
low grade (G1/G2)	85	87.6
high grade (G3/G4)	12	12.4
Histological classification		
adenocarcinoma	95	96.9
Mucinous adenocarcinoma	3	3.1

B

	pStat3 ^{high}	pStat3 ^{low}
pJak2 ^{high}	48	6
pJak2 ^{low}	14	30

p < 0.0001



F

	pStat3 ^{high}	pStat3 ^{low}
n = 50 p < 0.0001		
pJak2 ^{high}	28	1
pJak2 ^{low}	3	18

H

	p53 ^{mis}	53 ^{del}	p53 ^{wt}
n = 29 p < 0.00001			
p53 ^{high} /pStat3 ^{high}	13	1	0
p53 ^{low} /pStat3 ^{high}	0	3	2
p53 ^{high} /pStat3 ^{low}	7	0	0
p53 ^{low} /pStat3 ^{low}	0	0	3

G

p53 ^{high} / pStat3 ^{high}	p53 ^{low} / pStat3 ^{high}	p53 ^{high} / pStat3 ^{low}	p53 ^{low} / pStat3 ^{low}
3 x p.R248Q	p.W146*	p.R282W	wtp53
2 x p.R248W	p.R196*	p.R282W	wtp53
p.Y234N	wtp53	p.H178D	wtp53
p.A88S; p.Q298K; p.G776V	c.993+2T>C Ex7 skip	p.R280G	
c.994-2A>T Ex7 skip	wtp53	p.V173M	
p.T170M	p.T170M	p.R175H	
p.K132R		p.E258G	
p.R175H			
p.C135S			
p.D48Y			
p.R181H			

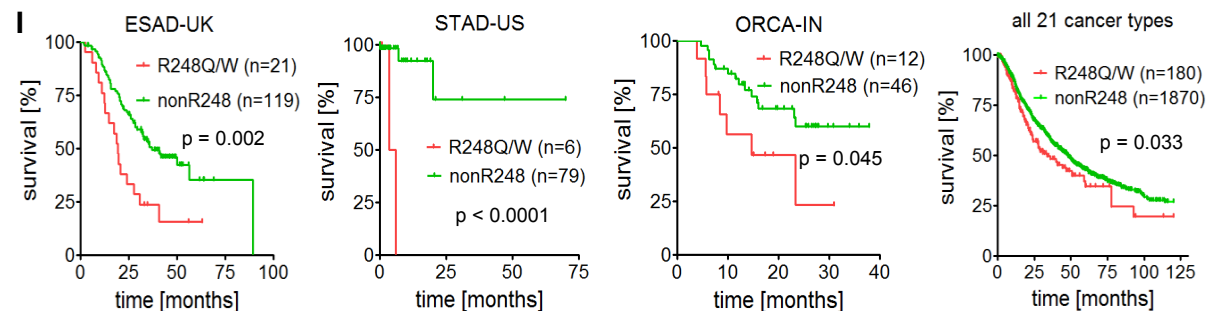


Figure S7. Related to Figure 7. mutp53 expression correlates with Jak2/Stat3 activation and poor survival in CRC patients. Cancer patients with $TP53^{R248Q/W}$ mutations have a higher death risk than all nonR248-mutant patients.

(A) Clinical characteristics of our CRC patient cohort and their tumors analyzed in Figures 7A-G and S7B-D.

(B) Correlation between pJAK2 and pStat3 in primary human colorectal carcinomas from patients in (A). n=98 cases, Fisher's exact test.

(C) Survival of CRC patients with primary tumors expressing pJak2^{high} or p53^{high}. (left) The median survival of patients with pJak2^{high} tumors is 56 months vs 72 months for patients with pJak2^{low} tumors. (right) Likewise, the median survival of patients with p53^{high} tumors is 58 months vs 77 months for patients with p53^{low} tumors. Kaplan-Meier Log-rank statistic. The same cohort as in Figures 7A-G was evaluated.

(D) Number of metastatic lymph nodes (LN) in CRC patients, separated by pUICC stage III vs IV. Even within the same tumor stage, patients with p53^{high}/pJak2^{high} or p53^{high}/pStat3^{high} primary CRC tumors have a higher number of metastatic LN.

For pUICC stage III, p53^{high}/pJak2^{high} (n = 13 patients) mean 5.9 LN vs p53^{low}/pJak2^{low} (n = 8 patients) mean 3.1 LN.

For pUICC stage IV, p53^{high}/pJak2^{high} (n = 12 patients) mean 3.3 LN vs p53^{low} /pJak2^{low} (n = 12 patients) mean 2.5 LN.

For pUICC stage III, p53^{high}/pStat3^{high} (n = 14 patients) mean 6.6 LN vs p53^{low}/pStat3^{low} (n = 7 patients) mean 3.7 LN.

For pUICC stage IV, p53^{high}/pStat3^{high} (n = 16 patients) mean 5.1 LN vs p53^{low}/pStat3^{low} (n = 7 patients) mean 2.6 LN.

Similar results were seen when patients were stratified by p53 expression alone. For pUICC stage III, p53^{high} (n = 17 patients) mean 7.9 LN vs p53^{low} (n = 13 patients) mean 3.1 LN. For pUICC stage IV, p53^{high} (n = 17 patients) mean 5.1 LN vs p53^{low} (n = 15 patients) mean 1.9 LN.

Same patient cohorts as in (B). Black lines, mean.

(E) p53 and pStat3 co-localize in human CRC tumor nuclei. Co-immunofluorescence staining with the indicated antibodies in a representative p53^{high}/pStat3^{high} tumor. Scale bar 100 μ m.

(F-H) *TP53* mutational analysis. Within our 98 patient CRC cohort, we analyzed a subgroup of 50 patients with resected CRC tumors and available material for DNA isolation. Again, in this subgroup the pJak2/pStat3 expression correlates nearly perfectly ($p < 0.0001$), i.e. the Jak2 status mirrors the Stat3 status in nearly all cases (F). Fisher's exact test. Among these 50 cases, we randomly chose 29 tumors for next generation sequencing (NGS) of *TP53*: 14 chosen out of 21 possible cases of the p53^{high}/Stat3^{high} group; 3 chosen out of 12 possible cases of the p53^{low}/Stat3^{low} group; 5 chosen out of 9 possible cases of the p53^{low}/Stat3^{high} group and 7 chosen out of 8 possible cases of the p53^{high}/Stat3^{low} group. The detected *TP53* mutations are listed (G). Importantly, in the p53^{high}/pStat3^{high} group there is an enrichment of the *TP53*^{R248Q/W} mutation (5/14 cases = 36%). Globally across all cancer entities, of all missense *TP53* mutations, *TP53*^{R248} mutations occur at a frequency of ~ 9%. Thus, the subgroup of pStat3^{high} expressing CRC tumors is specifically enriched for *TP53*^{R248} mutations, again supporting a mutp53-pStat3 axis. Conversely, in the p53^{low}/Stat3^{low} group, we only find WT *TP53* tumors (3/3 = 100%). Interestingly, the *TP53*^{R282W} mutation, which failed to form a strong Stat3 complex in HCT116 cells (Figure 6C), was only found in the p53^{high}/pStat3^{low} group. Finally in the p53^{low}/pStat3^{high} group, 3 out of the 5 cases show a p53 deletion mutation. WT p53 is known to suppress pStat3, and WT *TP53* deletion increases pStat3 levels (Lin et al., 2002; Wormann et al., 2016). (H) The *TP53* mutational analysis fully supports the p53/pStat3 staining correlations seen in Figure 7D. Correlation analysis yielded high significance in the Chi-Square test ($p < 0.00001$) and Fisher's Exact test ($p = 1.093 \times 10^{-6}$) between *TP53* mutational status and the p53/pStat3 expression status (H).

(I) Cancer patients with *TP53*^{R248} missense mutations have poorer survival compared to patients with all other nonR248 missense mutations. This is seen for many different cancer types. Kaplan-Meier survival analyses of the complete International Cancer Genome Consortium (ICGC) dataset, release # 25.

ICGC dataset ESAD-UK, esophageal carcinoma, the median survival of patients with *TP53*^{R248} mutations is 19.4 months vs 40.0 months in patients with nonR248 mutations.

ICGC dataset STAD-US, gastric cancer, the median survival of patients with $TP53^{R248}$ mutations is 4.7 months vs 75% survival beyond endpoint 70 months in patients with nonR248 mutations. ICGC dataset ORCA-IN, head & neck cancer, patients with $TP53^{R248}$ mutations have a median survival of 14.8 months vs 60% survival beyond endpoint 40 months in patients with nonR248 mutations. See also [Figures 7I, J](#). (right) In all assessable 21 primary cancer types from the ICGC datasets, the median survival of patients with $TP53^{R248}$ mutations is 33.6 months vs 48.0 months in patients with nonR248 mutations.

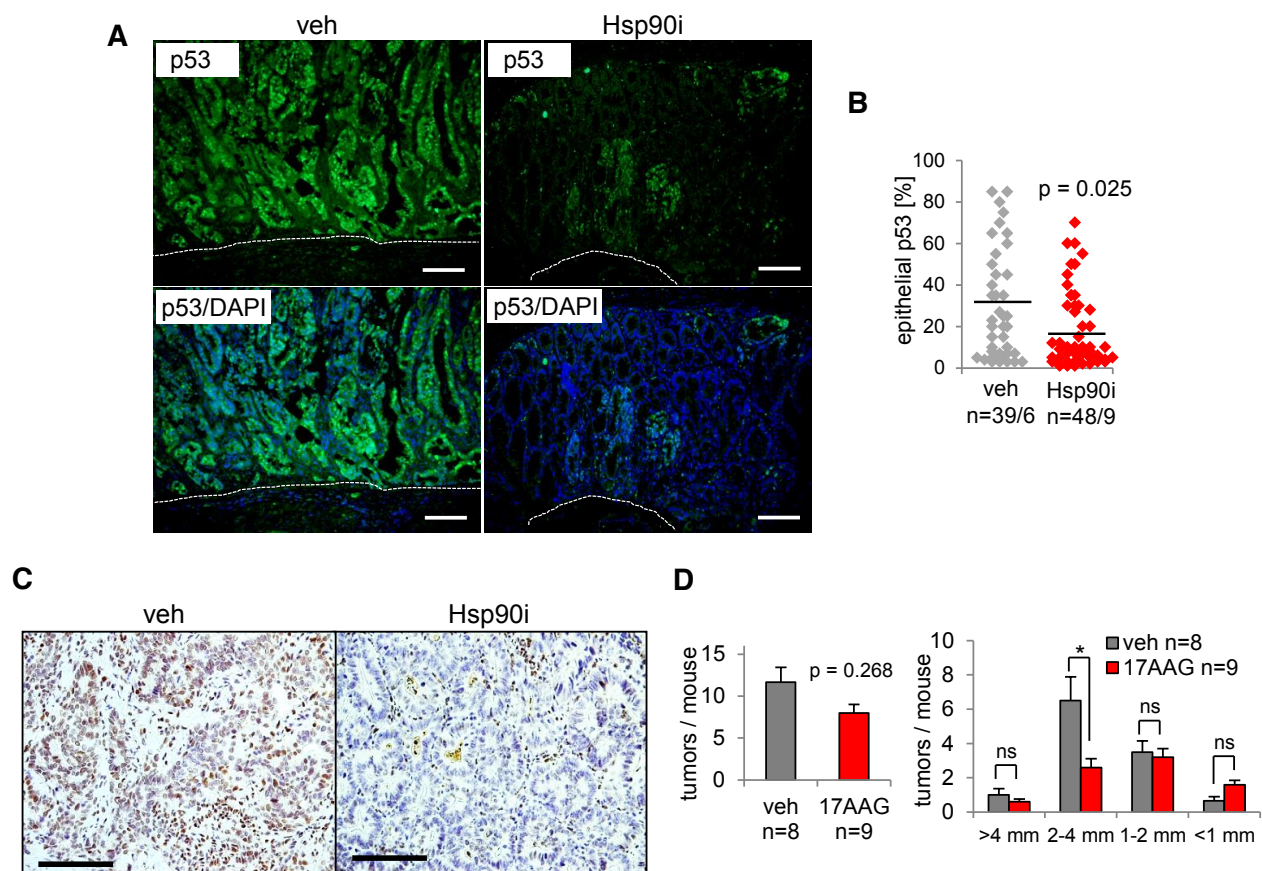


Figure S8. Related to Figure 8. **Pharmacological inhibition of Hsp90 reduces mutp53 levels and inhibits CRC tumors in mice.**

(A) Representative immunofluorescence staining for p53 (green) in p53^{Q/-} tumors after 4 weeks of vehicle or 17AAG (Hsp90i) treatment. DAPI counterstain for nuclei (blue). Dashed line, muscularis mucosae. Scale bars 100 μ m.

(B) Quantitation of tumor epithelial cells with p53-positive nuclei from the immunofluorescence analysis in (A). Two random fields at 40x magnification per tumor were counted. Positive nuclei as percentage of total epithelial nuclei are indicated. For vehicle 39 tumors from 6 mice and for Hsp90i 48 tumors from 9 mice were counted. Black lines indicate the mean. Student's t-test.

(C) Immunostaining of p53^{Q/-} tumors for pTyr705-Stat3 (pStat3) after treatment with vehicle or 17AAG for 4 weeks, indicating a decrease in the number of positive tumor nuclei. Scale bars 100 μ m.

(D) Tumor numbers (left) and size distribution (right) of p53^{-/-} control mice treated with vehicle or 17AAG for 4 weeks. Mean \pm SEM. Student's t-test. ns, not significant. n = number of mice.

Table S1, related to the STAR Methods. Primers for qPCR and genotyping.

Gene	Origin	Forward	Reverse
qPCR			
<i>CDH1</i>	Human	5'-CTTTGACGCCGAGAGCTACA	5'-AAATTCACTCTGCCAGGACG
<i>VIM</i>	Human	5'-CGTGTATGCCACGCGCTCCT	5'-TCGAGCTCGGCCAGCAGGAT
<i>MMP7</i>	Human	5'-GAGGAGCTCATGGGACTC	5'-CCATAGGTTGGATACATCACTGC
<i>SNAI1</i>	Human	5'-GCACATCCGAAGCCACAC	5'-GGAGAAGGTCCGAGCACAC
<i>MYC</i>	Human	5'-TACAACACCCGAGCAAGGAC	5'-AGCTAACGTTGAGGGGCATC
<i>CCNB1</i>	Human	5'-GAGCCAGTGCCAGGCCAGAA	5'-TTTCCAGTGACTTCCCAGCCAGT
<i>SOCS1</i>	Human	5'-TTTTCGCCCTTAGCGTGAA	5'-CATCCAGGTGAAAGCGGC
<i>SOCS3</i>	Human	5'-GGAGACTTCGATTCCGGACC	5'-GGTACTCGCTCTTGGAGCTG
<i>RPLP0</i> (36B4)	Human	5'-GATTGGCTACCCAATGTTG	5'-CAGGGGCAGCAGCCACAAA
<i>TP53</i>	Human	5'-AAGTCTAGAGCCACCGTCCA	5'-CAGTCTGGCTGCCAATCCA
<i>MUC1</i>	Human	5'-CTACCACAGCCCTAAACCC	5'-AGTAGTCGGTGTGGGATCT
<i>MMP2</i>	Human	5'-TACGATGGAGGCGCTAATGGC	5'-CACAAACAGGTTGCAGCTCTC
<i>Trp53</i>	Mouse	5'-GTGCTCACCCTGGCTAAAGT	5'-CAGTGAGGTGATGGCAGGAT
<i>Ccnd1</i>	Mouse	5'-GGAGCTGCTGCAATGGAAC	5'-CAGTCCGGGTCACTTGA
<i>Ccnb1</i>	Mouse	5'-CAGGGTCTGTAAGTACTGG	5'-GGCACACAAGTGTCTGCAT
<i>c-myc</i>	Mouse	5'-TTCTCTGCCTCTGCCCGTA	5'-TGAGGGGCATCGTCTGGCT
<i>Pcna</i>	Mouse	5'-AGTGGAGAGCTTGGCAATGG	5'-TCAGGTACCTCAGAGCAAACG
<i>Cdkn1a</i> (p21)	Mouse	5'-GTGGCCTTGTCTGTCTT	5'-GCGCTTGGAGTGATAGAAATCTG
<i>Cdkn2a</i> (p16)	Mouse	5'-CGCAGGTTCTTGGTCACTGT	5'-TTGCCCATCATCATCACCTGG
<i>Bbc3</i>	Mouse	5'-TTCTCCGGAGTGTTCATGCC	5'-ATACAGCGGAGGGCATCAGG
<i>Pmaip1</i> (Noxa)	Mouse	5'-CGGAACGCGCCAGTGAACCC	5'-GACTTCCCAGGCATCTGCGCC
<i>Cxcl1</i>	Mouse	5'-GACCATGGCTGGGATTCACC	5'-AGGGCAACACCTTCAAGCTC
<i>Cxcl2</i>	Mouse	5'-CTCTCAAGGGCGGTCAAAAAG	5'-TTGGTTCTTCCGTTGAGGGAC
<i>Socs1</i>	Mouse	5'-CGAGTAGGATGGTAGCACGC	5'-AAGGTGCGGAAGTGAGTGTCT
<i>Socs3</i>	Mouse	5'-TGTCGGAAGACTGTCAACGG	5'-AGGAAGAAGCCAATCTGCC
<i>RplpO</i> (36B4)	Mouse	5'-GCAGATCGGGTACCCAAGTGT	5'-CAGCAGCCGCAAATGCAGATG
genotyping			
<i>TP53</i> ^{R248Q/flox}	Mouse	5'-CCCTCCAGCTCAGCCTTTGTAG	5'-CTTGATCAAGGCTTGGAAAGC
<i>Trp53</i> (X6-X7) = WT	Mouse	5'-AGCGTGGTGGTACCTTATGAGC	5'-GGATGGTGGTATACTCAGAGCC
<i>Trp53</i> (neo-X7) = Del	Mouse	5'-GCTATCAGGACATAGCGTTGGC	~
<i>Rosa26CreERT2</i> = WT	Mouse	5'-AAA GTCGCTCTGAGTTGTTAT	5'-GGAGCGGGAGAAATGGA
<i>Rosa26CreERT2</i> = transgene	Mouse	5'-CCTGATCCTGGCAATTCG	~
<i>Apc</i> ^{1638N} = WT	Mouse	5'-CTAGCCCAGACTGCTTCAAAT	5'-GGAAAAGTTTATAGGTGTCCCTT
<i>Apc</i> ^{1638N} = Mut	Mouse	~	5'-GCCAGCTCATTCTCCACTC